Loss of pleckstrin-2 reverts lethality and vascular occlusions in JAK2[V617F]-positive myeloproliferative neoplasms

Baobing Zhao,[1,2] Yang Mei,[1,2] Lan Cao,[1,3] Jingxin Zhang,[1,2] Ronen Sumagin,[1,2] Jing Yang,[1,2] Juehua Gao,[1,2] Matthew J. Schipma,[4] Yanfeng Wang,[5,6] Chelsea Thorsheim,[5] Liang Zhao,[5] Timothy Stalker,[5] Brady Stein,[2,7] Qiang Jeremy Wen,[2,7] John D. Crispino,[2,7] Charles S. Abrams,[5] and Peng Ji[1,2]

[1]Department of Pathology, Feinberg School of Medicine, and [2]The Robert H. Lurie Comprehensive Cancer Center, Northwestern University, Chicago, Illinois, USA. [3]Department of Hematology and Oncology, Children's Hospital of Soochow University, Suzhou, China. [4]Center for Genetic Medicine, Northwestern University, Chicago, Illinois, USA. [5]Department of Medicine, University of Pennsylvania, Philadelphia, Pennsylvania, USA. [6]Zhongnan Hospital of Wuhan University, Wuhan, China. [7]Division of Hematology and Oncology, Department of Medicine, Northwestern University, Chicago, Illinois, USA.

V617F driver mutation of JAK2 is the leading cause of the Philadelphia-chromosome-negative myeloproliferative neoplasms (MPNs). Although thrombosis is a leading cause of mortality and morbidity in MPNs, the mechanisms underlying their pathogenesis are unclear. Here, we identified pleckstrin-2 (Plek2) as a downstream target of the JAK2/STAT5 pathway in erythroid and myeloid cells, and showed that it is upregulated in a JAK2[V617F]-positive MPN mouse model and in patients with MPNs. Loss of Plek2 ameliorated JAK2[V617F]-induced myeloproliferative phenotypes including erythrocytosis, neutrophilia, thrombocytosis, and splenomegaly, thereby reverting the widespread vascular occlusions and lethality in JAK2[V617F]-knockin mice. Additionally, we demonstrated that a reduction in red blood cell mass was the main contributing factor in the reversion of vascular occlusions. Thus, our study identifies Plek2 as an effector of the JAK2/STAT5 pathway and a key factor in the pathogenesis of JAK2[V617F]-induced MPNs, pointing to Plek2 as a viable target for the treatment of MPNs.

Introduction

Myeloproliferative neoplasms (MPNs) are a group of bone marrow diseases with excessive production of myeloid cells, increased risk of arterial or venous thrombosis, and a propensity to transform into acute myeloid leukemia. JAK2[V617F] mutation is the leading cause of the Philadelphia-chromosome-negative MPNs. Over 95% of the patients with polycythemia vera and 50%–60% of patients with essential thrombocythemia and primary myelofibrosis are JAK2[V617F] positive (1–4). The discovery of this driver mutation led to the development of JAK inhibitors for the treatment of MPNs. Reduction in spleen size and blood cell counts has been reported in MPN patients treated with JAK2 inhibitor (5, 6). However, distinct from the targeted therapy of BCR-ABL–positive chronic myelogenous leukemia, JAK2 is indispensable for normal hematopoiesis. Therefore, significant side effects including anemia and thrombocytopenia were inevitable when high doses were attempted (7). In addition, JAK2 inhibitor is not curative for the disease. Most patients with chronic JAK2 inhibitor treatment failed to reach molecular and pathologic remissions (6). Consistent with these observations, several reports showed variable efficacies of JAK2 inhibitors on the overall disease burden in mouse

models (7, 8). These studies indicate that targeting JAK2 alone may not be sufficient to treat the disease.

Nevertheless, gene expression profile analysis demonstrated that regardless of the JAK2 mutational status, patients with Philadelphia-chromosome-negative MPNs are characterized by a distinct gene expression profile with upregulation of JAK/STAT downstream genes (9). More recent studies further confirmed that patients with calreticulin or myeloproliferative leukemia virus oncogene (MPL) mutations, the other 2 major genetic abnormalities in Philadelphia-chromosome-negative MPNs (10), also involve activation of the JAK/STAT pathway (11). These reports underscore the JAK/STAT pathway in the pathogenesis of MPNs and as a valid target for therapy. Several studies started to explore the combined targeting of JAK2 and JAK/STAT pathway downstream effectors to achieve molecular remission or overcome resistance to JAK2 inhibitors. For example, combined targeting of Bcl-xL and JAK2 has shown to be more effective than a JAK2 inhibitor alone in JAK2[V617F]-driven malignancy in a mouse model (12). A Bcl-xL inhibitor was also combined with interferon α to specifically target JAK2[V617F]-positive hematopoietic progenitor cells (13). Furthermore, pimozide, a STAT5 inhibitor, was reported to be effective in cell lines or primary cells by itself or in combination with a JAK2 inhibitor (14, 15).

Pleckstrin-2 (Plek2) is a widely expressed paralog of pleckstrin-1 (Plek1) and is involved in actin dynamics (16). We previously discovered that Plek2 plays important roles in erythroblast survival and enucleation in the early and late stages of terminal erythropoiesis, respectively (17). In that report, we also found that the Plek2 level is

responsive to erythropoietin (Epo). Here we show that Plek2 is a target of the JAK2/STAT5 pathway. Plek2 is upregulated in JAK2[V617F]-transduced primary hematopoietic cells and in JAK2[V617F]-positive MPN patients. We demonstrate that loss of Plek2 substantially ameliorated the myeloproliferative phenotypes in a JAK2[V617F]-knockin mouse model. More importantly, loss of Plek2 rescued the widespread vascular occlusions and lethality of JAK2[V617F]-knockin mice, mainly through the reduction of whole-body red blood cell (RBC) mass. Therefore, we provide genetic evidence that Plek2 is essential for the pathogenesis of JAK2[V617F]-induced MPNs, and a rationale for targeting Plek2 for the treatment of JAK2[V617F]-positive MPNs.

Results

Epo-dependent transcriptional regulation of Plek2. To determine the mechanisms underlying how Plek2 expression is regulated, we purified erythroblasts negative for Ter119 (a maturing erythroid cell surface marker) from embryonic day 13.5 (E13.5) mouse fetal liver and cultured them in Epo-containing medium for 2 days (18, 19). Plek2 levels gradually increased and reached a peak on day 1, and gradually decreased on day 2 (Figure 1A). We then cultured the purified Ter119-negative fetal liver cells in stem cell factor–containing (SCF-containing) medium for 12 hours to eliminate the influence of endogenous Epo. These cells were subsequently changed into Epo-containing medium. Compared with the cells cultured without Epo, cells exposed to Epo showed a substantial upregulation of Plek2 protein level (Figure 1B). The influence of Epo on Plek2's expression was rapid in that cells cultured for approximately 9 hours in Epo-containing medium already exhibited a substantial Plek2 upregulation (Figure 1C). We further analyzed the Plek2 expression at specific stages of mouse terminal erythropoiesis by utilizing an intracellular flow cytometric assay. Erythroid differentiation was determined by CD44 expression since it is known to gradually decrease during erythroid terminal maturation (20) (Figure 1D). Consistent with our immunoblotting experiments, Plek2 gradually increased in the early stages of differentiation and then decreased as the cells continued to mature (Figure 1E). We further observed that Epo-induced Plek2 upregulation was mediated by the regulation of transcription (Figure 1, F and G). In contrast to Plek2, Epo had no effect on the expression of Plek1 (Figure 1, H and I). These experiments establish a transcriptional regulation of Plek2 expression that is Epo dependent.

Plek2 is a downstream target of the JAK2/STAT5 pathway. The most well-known mediator of Epo signaling is the JAK2/STAT5 pathway (21). To analyze whether Plek2 expression is regulated through the JAK2/STAT5 pathway, we treated Ter119-negative fetal liver erythroid cells with JAK2 inhibitors and cultured them in Epo-containing medium for 24 hours. In a dose-dependent pattern, the JAK2 inhibitors AZD1480 and ruxolitinib inhibited the protein and mRNA expression of Plek2 (Figure 2, A and B). However, the level of Plek1 was not affected, demonstrating that the pleckstrin family proteins are differentially regulated during erythropoiesis (Supplemental Figure 1A; supplemental material available online with this article; https://doi.org/10.1172/JCI94518DS1). Plek1 protein levels slightly increased with the downregulation of Plek2, possibly compensating for the acute loss of Plek2 (Figure 2A).

Having demonstrated a relationship between the loss of JAK2 activity and Plek2 expression, we analyzed whether a gain of function within JAK2 would increase Plek2 expression. This was done by transducing Ter119-negative bone marrow cells with a retroviral construct that directed the expression of JAK2[V617F]. We observed that JAK2[V617F] induced upregulation of Plek2 and phosphorylation of STAT5 (Figure 2, C and D). As expected, a constitutively active STAT5 mutant, but not the wild-type STAT5 or a dominant-negative mutant, also substantially induced Plek2 expression (Figure 2, E and F). Since JAK2 signaling also plays critical roles in the differentiation and proliferation of other myeloid lineages such as megakaryocytes and granulocytes, we next tested Plek2 expression in these lineages. Indeed, Plek2 protein and mRNA upregulation was also observed when the lineage-negative bone marrow cells were induced to differentiate into the megakaryocytic (Figure 2, G and H) or granulocytic lineages (Figure 2, I and J).

To directly demonstrate that Plek2 is a downstream target of the JAK2/STAT5 pathway, we performed a chromatin immunoprecipitation (ChIP) assay using a polyclonal antibody against STAT5. Several STAT5 consensus-binding sites are present in the promoter region of *Plek2* (Supplemental Figure 1B). By sequentially using ChIP followed by quantitative PCR, we found that STAT5 bound preferentially to the STAT5 consensus-binding sites most proximal to the start codon of *Plek2* (Figure 2K). A luciferase assay showed a marked increase of luciferase activity in cells transduced with a constitutively active STAT5 mutant and the *Plek2* promoter, confirming the functional role of JAK2/STAT5 in regulating Plek2 expression (Figure 2L). We further analyzed the *Plek2* promoter region using published ATAC (assay for transposase-accessible chromatin) sequencing data (22) and revealed the high chromatin accessibility of the *Plek2* locus leading to cell type–specific expression in erythroid cells compared with other cell lineages (Figure 2, M and N), which is similar to hemoglobin genes (Supplemental Figure 1, C and D). Taken together, these data establish that Plek2 is a transcriptional target of the JAK2/STAT5 signaling pathway.

The functions of Plek2 under steady-state hematopoiesis. Our previous study showed that Plek2 is critical for both the early and late stages of terminal erythropoiesis in vitro in cultured mouse fetal liver erythroid cells (17). However, the role of Plek2 in vivo is unknown. Therefore, we generated a Plek2 whole-body conventional knockout mouse model. Depletion of Plek2 in bone marrow mononuclear cells was confirmed by Western blot analysis, which also showed that there was no significant compensatory upregulation of Plek1 in vivo (Figure 3A). Plek2-knockout mice did not exhibit hematologic abnormalities at young ages (2–4 months old) but developed statistically significant, albeit very minor anemia when the mice were over 1 year of age (Figure 3B). Older (>1 year of age) Plek2-knockout mice also developed mild ineffective erythropoiesis demonstrated by slightly increased erythroblasts and decreased reticulocytes in bone marrow compared with wild-type controls (Figure 3C). Minor changes were also present in the spleens of Plek2-knockout mice, and their spleens were slightly enlarged (Figure 3, D and E). Other lineages of the hematopoietic cells were not affected in the older Plek2-knockout mice (Figure 3F). Consistent with our prior study that demonstrated that Plek2 is critical in the regulation of oxidative damage in terminal erythropoiesis in vitro (17), we found that the peripheral RBC of Plek2-
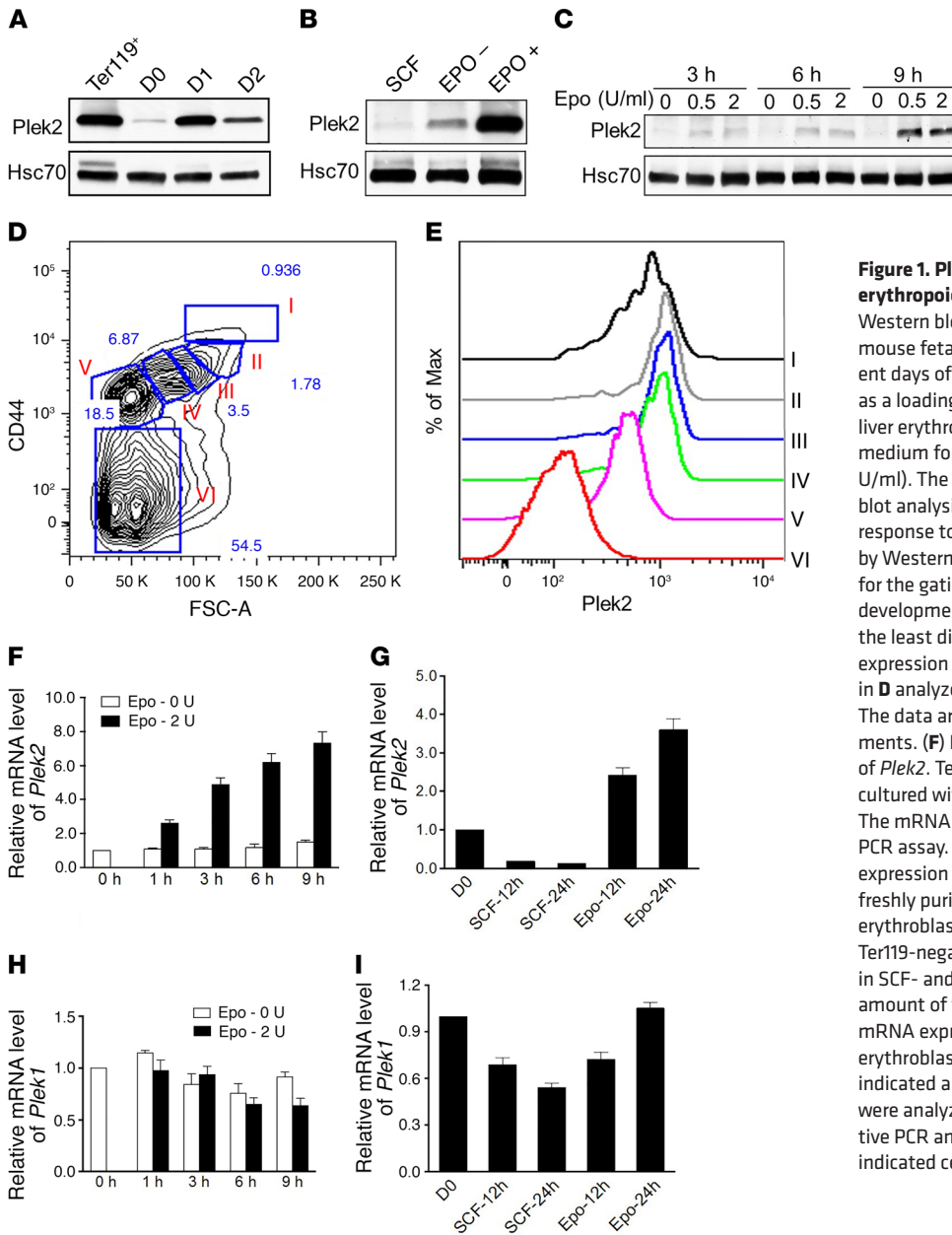
Figure 1. Plek2 is transcriptionally regulated by erythropoietin. (**A**) The level of Plek2 was detected by Western blot analysis. Ter119$^+$ indicates Ter119-positive mouse fetal liver erythroblasts. D1 to D3 indicate different days of mouse fetal liver culture. Hsc70 was used as a loading control. (**B**) Ter119-negative mouse fetal liver erythroblasts were cultured in SCF-containing medium followed by culture with or without Epo (2 U/ml). The levels of Plek2 were detected by Western blot analysis. (**C**) Time course of Plek2 expression in response to Epo. The levels of Plek2 were detected by Western blot analysis. (**D**) Flow cytometric assay for the gating of erythroid populations in different developmental stages. Populations I to VI represent the least differentiated to enucleated RBC. (**E**) Plek2 expression in different populations of erythroblasts as in **D** analyzed by an intracellular flow cytometric assay. The data are representative of 3 independent experiments. (**F**) Epo drives the transcriptional upregulation of *Plek2*. Ter119-negative fetal liver erythroblasts were cultured with or without Epo for the indicated period. The mRNA levels of *Plek2* were analyzed by a real-time PCR assay. (**G**) Quantitative PCR analysis of the mRNA expression of *Plek2* in indicated cells. D0 indicates freshly purified Ter119-negative mouse fetal liver erythroblasts. SCF-12h, -24h and Epo-12h, -24h indicate Ter119-negative mouse fetal liver erythroblasts cultured in SCF- and Epo-containing medium for the indicated amount of time, respectively. (**H**) Effects of Epo on the mRNA expression of *Plek1*. Ter119-negative fetal liver erythroblasts were cultured with or without Epo for the indicated amount of time. The mRNA levels of *Plek1* were analyzed by a real-time PCR assay. (**I**) Quantitative PCR analysis of the mRNA expression of Plek1 in indicated cells as in **G**.

knockout mice exhibited an increased sensitivity to oxidative damage (Figure 3, G and H). This suggests that Plek2 may have a protective effect on RBC integrity in an oxidative environment in vivo. Together, these data demonstrate that Plek2 does not significantly contribute to steady-state hematopoiesis in vivo.

To further determine the role of Plek2 in vivo, we transplanted Plek2-overexpressing bone marrow cells into lethally irradiated recipient mice. Western blot assay of total bone marrow cells from recipient mice 2 months after transplantation confirmed Plek2 overexpression (Figure 3I). These mice showed mild increases in RBC indices as well as platelet count. The white blood cell (WBC) count remained unchanged (Figure 3J). Bone marrow analysis revealed no overt effects in Plek2-overexpressing hematopoietic stem and progenitor cells (data not shown). When we cultured the bone marrow lineage-negative cells from these mice in vitro in Epo-containing medium, Plek2-overexpressing cells showed an

increased proliferation rate compared with the vector control mice (Figure 3K). These studies further confirm the mild in vivo functions of Plek2 under steady state and its possible pro-proliferative ability in erythroid cells.

Plek2 is significantly upregulated by JAK2^{V617F} in MPN patients and mice. Many genes reveal their in vivo phenotypes only under disease conditions. Since Plek2 is a downstream target of JAK2, we analyzed whether Plek2 is a necessary component of a critical signaling pathway required for the pathogenesis of JAK2^{V617F}-induced MPN. We first analyzed the published next-generation sequencing data from patients with JAK2^{V617F}-positive MPNs (23–29). As expected, Plek2 is significantly upregulated in bone marrow samples obtained from 16 JAK2^{V617F}-positive polycythemia vera patients and 9 JAK2^{V617F}-positive essential thrombocythemia patients compared with the corresponding normal individuals (Figure 4A). An independent assay using mononuclear cells from
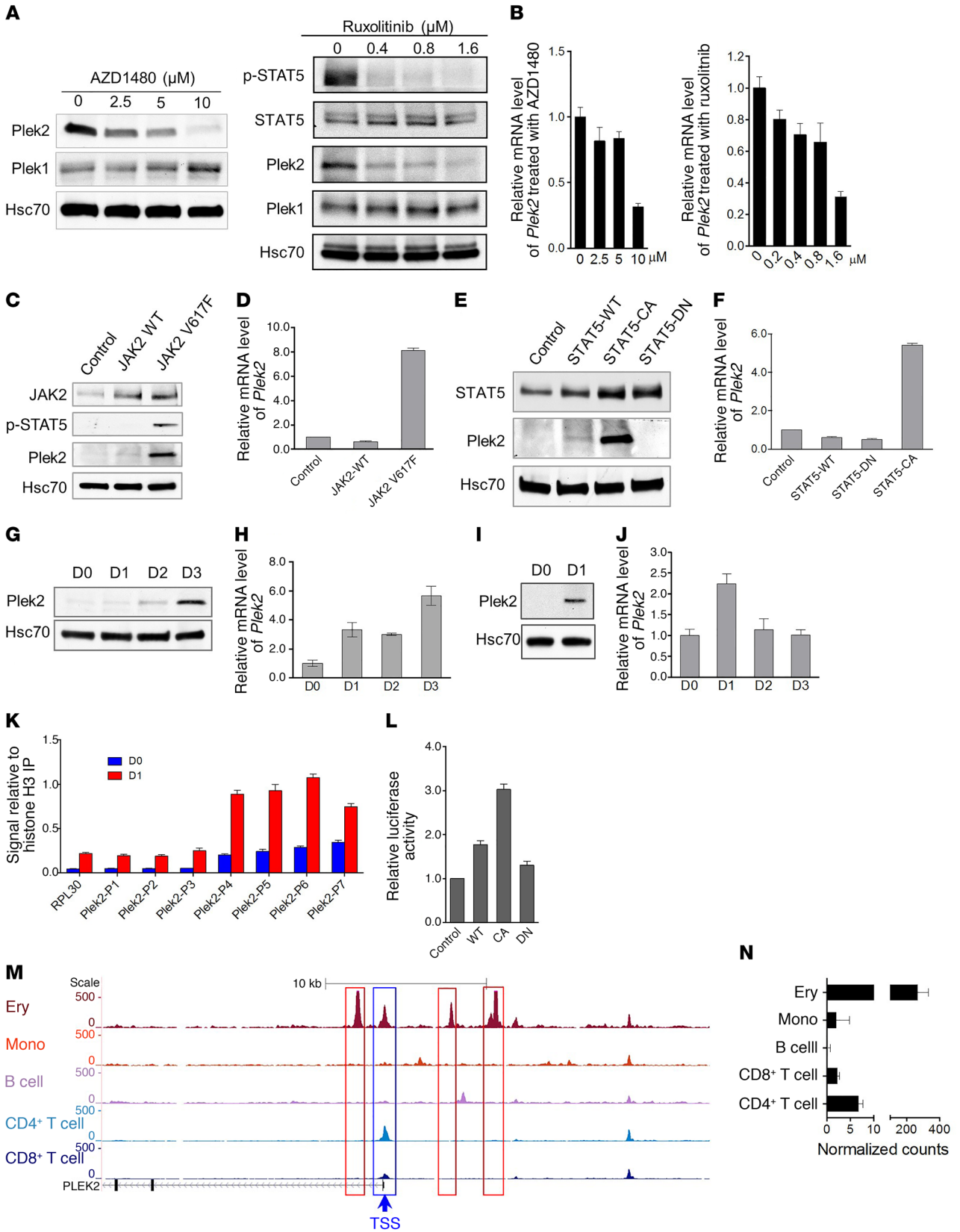
Figure 2. Plek2 is a downstream target of the JAK2/STAT5 pathway. (**A** and **B**) Western blot (**A**) and quantitative PCR (**B**) analyses of Plek2 expression in the cultured erythroblasts treated with indicated JAK2 inhibitors after 20 hours. Different concentrations of JAK2 inhibitor AZD1480 or ruxolitinib were added to the cultured erythroblasts in the presence of Epo (2 U/ml). Hsc70 was used as a loading control. (**C** and **D**) Western blot (**C**) and quantitative PCR (**D**) analyses of Plek2 expression in the cultured erythroblasts transduced with JAK2 wild-type (WT) and JAK2^{V617F} mutant. (**E** and **F**) Western blot (**E**) and quantitative PCR (**F**) analyses of Plek2 expression in the cultured erythroblasts transduced with STAT5 wild-type (WT), dominant-negative (DN), and constitutively active (CA) mutants. (**G** and **H**) Western blot (**G**) and quantitative PCR (**H**) analyses of Plek2 expression in the cultured lineage-negative bone marrow progenitor cells exposed to thrombopoietin. D1 to D3 indicate different days of in vitro culture. (**I** and **J**) Same as **G** and **H** except the cells were exposed to GM-CSF. (**K**) ChIP–quantitative PCR assay showing STAT5 binding at the *Plek2* promoter in freshly purified Ter119-negative E13.5 mouse fetal liver erythroblasts (D0) and cultured mouse fetal liver erythroblasts on day 1 (D1). P1 to P7 indicate fragments in the *Plek2* promoter region amplified in ChIP–qPCR assays. (**L**) Luciferase reporter assay of STAT5 binding on the *Plek2* promoter. HET293T cells were transfected with indicated constructs, together with a *Plek2* promoter construct. Luciferase activity was measured at 48 hours after transfection. (**M** and **N**) Normalized ATAC-sequencing peaks in the *Plek2* locus (**M**) and relative expression of *Plek2* (**N**) in the indicated cell type. Ery, erythroid cells; Mono, monocyte. The *y* axis represents normalized arbitrary units. Boxed regions show cell type–specific peaks around the *Plek2* gene. TSS, transcription start site. Data were obtained from Corces et al. (22).

the peripheral blood of 16 JAK2^{V617F}-positive MPN patients with different diseases including myelofibrosis revealed a significant upregulation of Plek2 protein and mRNA levels (Figure 4, B and C). Furthermore, immunohistochemical stains of the bone marrow core biopsy also showed pan-myeloid increased expression of Plek2 in JAK2^{V617F}-positive MPN patients (Figure 4D). These data confirm the increased expression of Plek2 and indicate its possible role in the pathogenesis of JAK2^{V617F}-induced MPNs.

We next utilized a mouse genetic approach with a JAK2^{V617F} hematopoietic-specific knockin mouse model (JAK2 V617F$^{fl/+}$/Vav-Cre, hereafter referred to as JAK2^{V617F} mice) that closely mimics the pathogenesis in human MPN patients (30). We first analyzed *Plek2* mRNA expression in the specific bone marrow hematopoietic lineages and observed that Plek2 was upregulated in both myeloid and lymphoid cells, but most strongly in erythroid cells, in JAK2^{V617F}-knockin mice (Figure 4E). To determine the contribution of Plek2 to the pathogenesis of JAK2^{V617F}-induced MPNs, we paired Plek2-knockout mice with JAK2^{V617F} mice and generated JAK2 V617F$^{fl/+}$/Vav-Cre/Plek2$^{-/-}$ mice (which will be referred to as JAK2$^{VF/+}$ Plek2$^{-/-}$) with their littermate controls. Western blot analyses performed on bone marrow erythroid, megakaryocytic, and granulocytic cells showed a substantial upregulation of Plek2 in JAK2$^{VF/+}$ Plek2$^{+/+}$ mice, whereas Plek2 was undetectable in JAK2$^{+/+}$ Plek2$^{-/-}$ and JAK2$^{VF/+}$ Plek2$^{-/-}$ mice (Figure 4F).

Loss of Plek2 ameliorates JAK2^{V617F}-induced myeloproliferative phenotypes. As previously reported (30), JAK2$^{VF/+}$ Plek2$^{+/+}$ mice showed erythrocytosis, leukocytosis (including neutrophilia), and thrombocytosis (Figure 5A). Reticulocytes were also significantly increased, further reflecting the hyperproliferation of the erythroid lineage (Figure 5B and Supplemental Figure 2A). Consistent with the role of Plek2 in mediating JAK2 signaling in various myeloid lineages, loss of Plek2 significantly reverted the JAK2^{V617F}-mediated neutro-

philia and thrombocytosis, mildly reduced RBC count (Figure 5A), and partially reverted reticulocytosis (Figure 5B and Supplemental Figure 2A). Several proinflammatory cytokines that were reported to be upregulated in JAK2^{V617F}-knockin mice (31), including MIP-1a (also known as CCL3) and CSF1, were significantly reduced. This is consistent with the reduction of WBC, since they are a major source of these cytokines (Supplemental Figure 2B).

In mice, the JAK2^{V617F} knockin has been previously described to induce erythroid and megakaryocytic hyperplasia within the bone marrow and spleen, analogous to humans with JAK2^{V617F} MPNs (30). Therefore, we analyzed whether loss of Plek2 would revert the bone marrow and spleen histology in JAK2$^{VF/+}$ Plek2$^{+/+}$ mice. We observed that JAK2$^{VF/+}$ Plek2$^{-/-}$ mice had significantly fewer megakaryocytes and fewer megakaryocyte clusters than JAK2$^{VF/+}$ Plek2$^{+/+}$ mice (Figure 5, C and D). Compared with JAK2$^{VF/+}$ Plek2$^{+/+}$ spleens, the size of the JAK2$^{VF/+}$ Plek2$^{-/-}$ spleens was reduced, although extramedullary hematopoiesis was still present (Figure 5, C and E). Consistent with the previous report (30), JAK2$^{VF/+}$ Plek2$^{+/+}$ mice did not develop myelofibrosis at the moribund stage, although the blood cell counts and Plek2 level remained high (Supplemental Figure 3, A–C).

Reduction of RBC mass in JAK2^{V617F}-knockin mice with the loss of Plek2. Splenomegaly is one of the key features of MPNs. The expanded red pulps in the enlarged spleen serve as a RBC reservoir and contribute significantly to the whole-body RBC mass (10). The reduced spleen size in JAK2$^{VF/+}$ Plek2$^{-/-}$ mice indicates that loss of Plek2 might reduce whole-body RBC mass, which cannot be accurately evaluated using peripheral blood RBC count.

To demonstrate the reduction of RBC mass with the loss of Plek2 in JAK2^{V617F}-knockin mice, we investigated the blood vessels in these mice. Consistent with a previous report (32), JAK2^{V617F}-knockin mice showed enlarged diameters of the mesenteric vessels and aortic area that may reflect a process of adaptation to the increased RBC mass. As expected, loss of Plek2 significantly reduced the diameters of mesenteric vessels and aortic area, which is consistent with a reduction of whole-body RBC mass in JAK2$^{VF/+}$ Plek2$^{-/-}$ mice (Figure 6, A–C). We further measured the blood volume in these mice and calculated circulating RBC mass. Similar to previous reports, we found that the presence of the JAK2^{V617F} mutation roughly tripled the RBC mass by increasing the absolute whole-body RBC number by approximately 4×10^{10}. We observed that loss of Plek2 reverted approximately 25% of the RBC expansion induced by the JAK2^{V617F} mutation (Figure 6, D and E).

To further confirm the role of Plek2 in the JAK2/STAT5 signaling pathway in the JAK2^{V617F}-knockin mouse model, we performed ex vivo cell proliferation and differentiation assays using purified bone marrow lineage-negative cells from these mice. To this end, we cultured the lineage-negative hematopoietic stem and progenitor cells from JAK2$^{VF/+}$ Plek2$^{+/+}$, JAK2$^{VF/+}$ Plek2$^{-/-}$, or their littermate controls, in a medium containing SCF but without Epo or GM-CSF. The cells were cultured for 2 days and purified a second time to ensure that the progenitors were completely free of the influence of Epo or GM-CSF in vivo. These cells were then placed into media containing Epo or GM-CSF to induce their differentiation to the erythroid or granulocytic lineage, respectively. Indeed, loss of Plek2 substantially reduced the increased proliferation of erythroid (Figure 6F) and granulocytic (Figure 6G) cells from JAK2$^{VF/+}$ Plek2$^{+/+}$ mice.
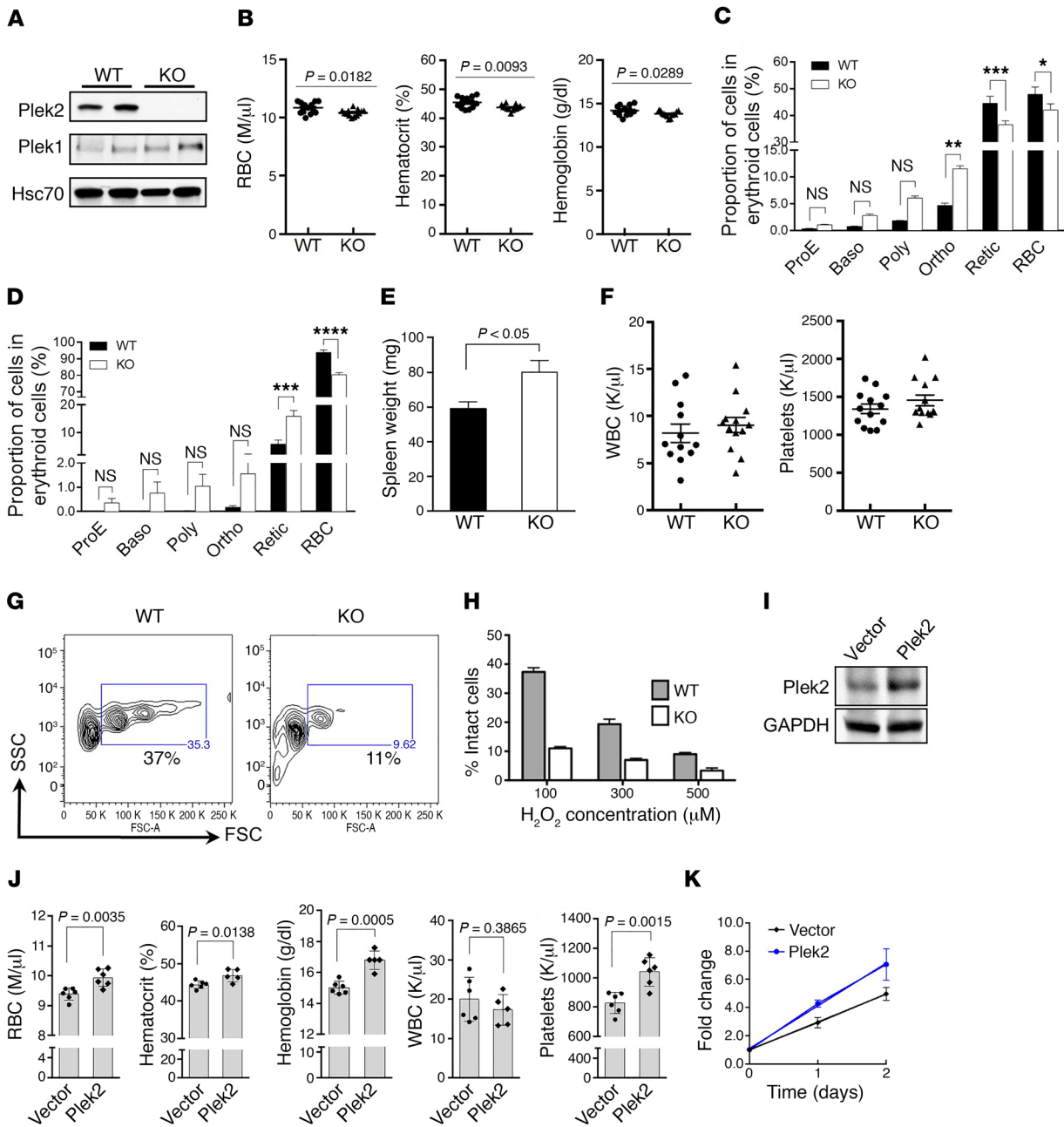
Figure 3. Plek2-knockout mice exhibit a mild anemia with aging. (**A**) Western blot analysis of Plek2 and Plek1 of bone marrow mononuclear cells from the indicated mice. Hsc70 was used as a loading control. (**B**) RBC indices (in millions [M] of cells per μl) of indicated mice at 1 year old. N = 13/group. P value was determined by 2-tailed t test. (**C** and **D**) Quantification of different stages of erythroblasts by flow cytometric analyses from bone marrow (**C**) and spleen (**D**) of indicated mice at 1 year old. ProE, proerythroblasts; Baso, basophilic erythroblasts; Poly, polychromatic erythroblasts; Ortho, orthochromatic erythroblasts; Retic, reticulocytes. N = 5/group. *P < 0.05, **P < 0.01, ***P < 0.0005, and ****P < 0.0001; all P values were determined by 2-way ANOVA with Sidak's multiple comparisons test. (**E**) Quantification of spleen weight of indicated mice at 1 year old. N = 5/group. P value was determined by 2-tailed t test. (**F**) Peripheral blood count of WBC (in thousands [K] of cells per μl) and platelets in indicated mice at 1 year old. (**G**) Flow cytometric assay of RBC from Plek2 wild-type and knockout mice treated with 100 μM H_2O_2 for 12 hours. The percentages of forward scatter–high (FSC-high) intact erythrocytes are presented. (**H**) Quantitative analysis of **G** at different concentrations of H_2O_2. (**I**) Western blot analysis of bone marrow cells from mice transplanted with Plek2-overexpressing bone marrow for 2 months. GAPDH was used as a loading control. (**J**) Complete blood count of mice transplanted with Plek2-overexpressing bone marrow for 2 months. P values were determined by 2-tailed t test. (**K**) Bone marrow lineage-negative cells from the indicated transplanted mice were purified and cultured in vitro in erythropoietin-containing medium. The cell numbers were counted at the indicated time. N = 3/group.
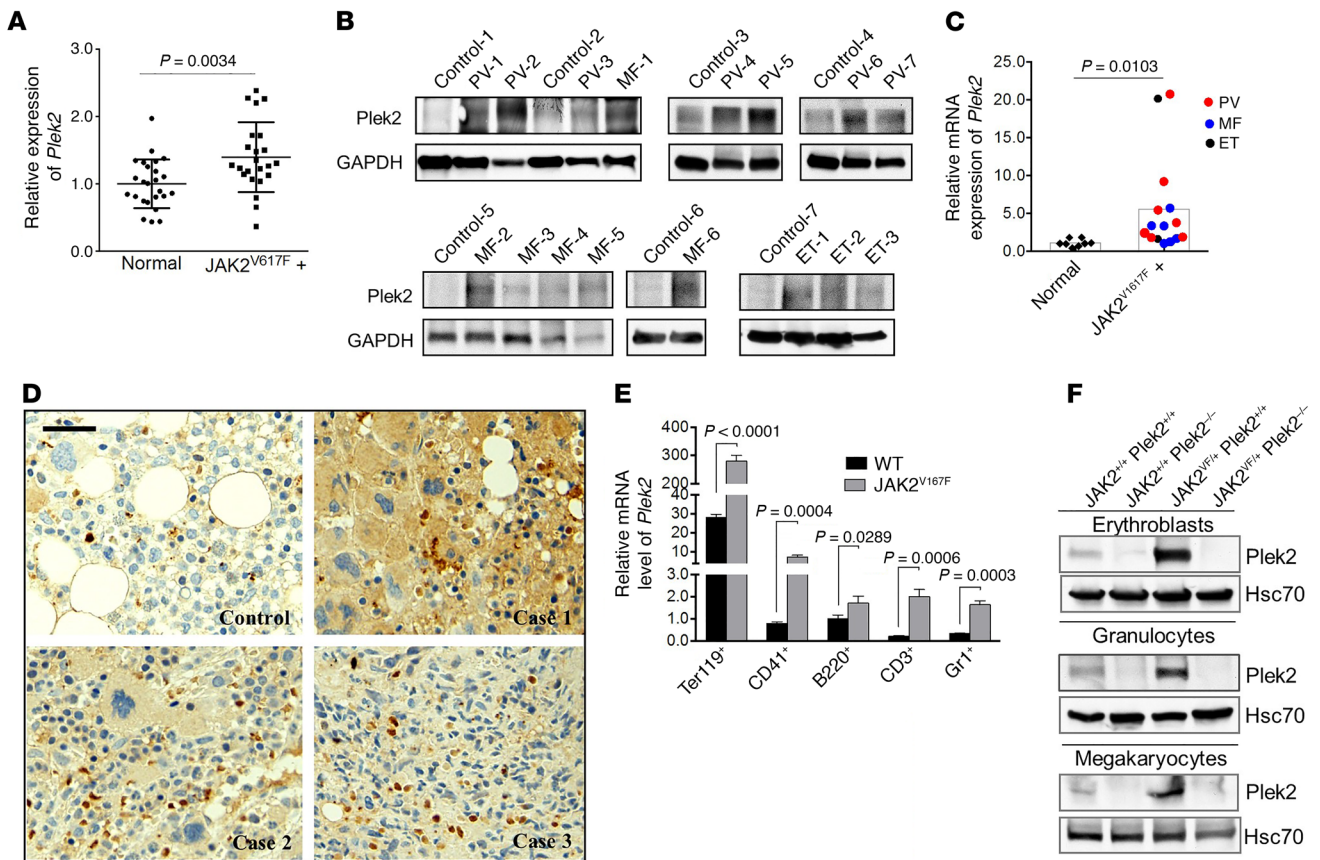
Figure 4. Plek2 is significantly upregulated by JAK2^{V617F} in mice and MPN patients. (**A**) Gene expression levels of *Plek2* in samples derived from 16 JAK2^{V617F}-positive PV patients and 9 JAK2^{V617F}-positive ET patients relative to the corresponding normal individuals (*n* = 26). Data were obtained from Berkofsky-Fessler et al. (24) and Puigdecanet et al. (28). *P* value was determined by 2-tailed *t* test. (**B**) Western blot analysis of Plek2 in the peripheral blood nucleated cells from 16 JAK2^{V617F}-positive MPN patients with different diseases and 8 normal control patients. GAPDH is the loading control. PV, polycythemia vera; MF, myelofibrosis; ET, essential thrombocythemia. (**C**) Relative gene expression of *Plek2* in samples from **B**. Mononuclear cells were purified from these samples followed by quantitative PCR analysis. *P* value was determined by 2-tailed *t* test. (**D**) Immunohistochemical stains of Plek2 in bone marrow core biopsies from 3 cases of JAK2^{V617F}-positive MPN and 1 healthy control individual. Scale bar: 50 μm. (**E**) Quantitative RT-PCR assay of relative mRNA expression levels of *Plek2* in different bone marrow hematopoietic lineages from wild-type and JAK2^{V617F}-knockin mice. *P* values were determined by 2-tailed *t* test. (**F**) Western blot analyses of Plek2 in erythroblasts, granulocytes, and megakaryocytes from the bone marrow of indicated mice. Hsc70 was used as a loading control.

Erythroid differentiation to Ter119/CD71 double-positive cells (Supplemental Figure 4A), granulocytic differentiation to Gr1/Mac1 double-positive cells (Supplemental Figure 4B), and early-stage megakaryocytic differentiation to CD41-positive cells (Supplemental Figure 4C) were also mildly decreased in cells from JAK2$^{+/+}$ Plek2$^{-/-}$ and JAK2$^{VF/+}$ Plek2$^{-/-}$ mice cultured in vitro. In addition, the effect of the JAK2$^{VF/+}$ mutation on ex vivo chemokine-induced neutrophil migration was reverted in JAK2$^{VF/+}$ Plek2$^{-/-}$ mice (Supplemental Figure 5A). However, ex vivo analyses of platelet aggregation did not detect significant differences (Supplemental Figure 5B) between the JAK2$^{VF/+}$ Plek2$^{-/-}$ and JAK2$^{VF/+}$ Plek2$^{+/+}$ mice, although we did observe small differences in platelet secretion between these 2 groups of mice. Flow cytometric analysis of bone marrow stem cell populations revealed that the JAK2^{V617F} mutation did not affect the compositions of long-term hematopoietic stem cells (HSCs), short-term HSCs, or multipotent progenitors (MPPs), but induced expansion of the megakaryocytic and erythroid progenitor population (MEP) within myeloid progenitor cells (lineage$^-$Sca1$^-$c-kit$^+$), which is consistent with previ-

ous reports (30). Loss of Plek2 had no further influence on these populations (Supplemental Figure 6, A and B). Taken together, these results demonstrate that the rescue of JAK2^{V617F} myeloproliferative phenotypes by the loss of Plek2 may be primarily due to the amelioration of the hyperproliferation in the erythroid and myeloid lineages. This model was confirmed by using shRNA to knock down Plek2 in the human SET-2 cell line that harbors the JAK2^{V617F} mutation, and demonstrated a substantial decrease in cell proliferation by the loss of Plek2 (Figure 6, H and I).

Loss of Plek2 reverted JAK2^{V617F}-induced vascular occlusion and lethality. We followed these mice for up to 40 weeks. All the JAK2$^{VF/+}$ Plek2$^{+/+}$ mice died at around 30 weeks of age, whereas more than 80% of the JAK2$^{VF/+}$ Plek2$^{-/-}$ mice survived beyond 40 weeks (Figure 7A). We also transplanted the bone marrow cells from JAK2$^{VF/+}$ Plek2$^{+/+}$, JAK2$^{VF/+}$ Plek2$^{-/-}$, or their littermate control mice into lethally irradiated recipient mice. Flow cytometric analyses showed successful engraftment with no difference in the percentage of donor chimerism across different genotypes (data not shown). The mice transplanted with JAK2$^{VF/+}$ Plek2$^{-/-}$ bone marrow exhibited
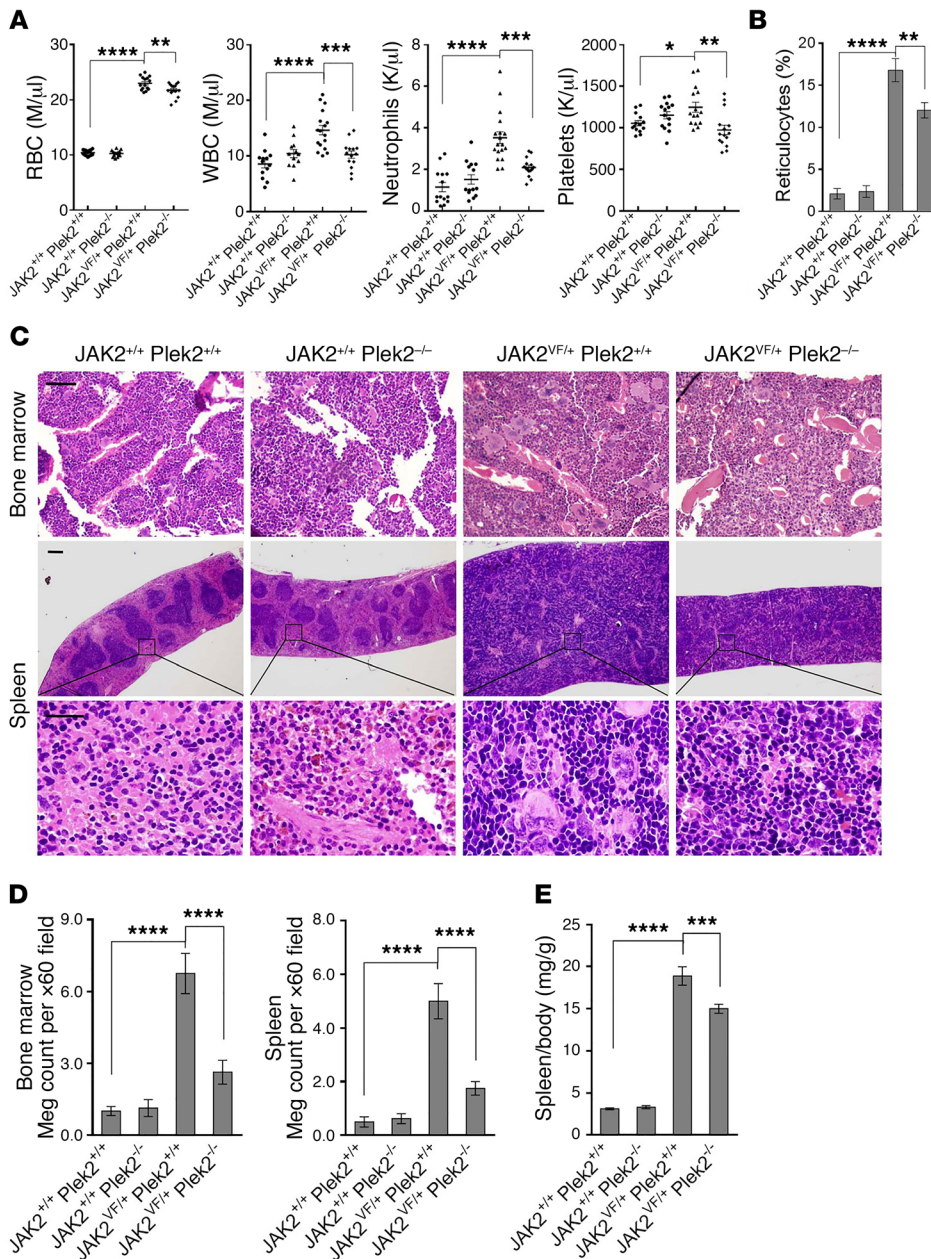
Figure 5. Loss of Plek2 ameliorates JAK2^{V617F}-induced myeloproliferative phenotypes. (**A**) Complete blood counts of the indicated mice. Both males and females at the age of 3–4 months were included. Each data point represents 1 mouse. M, millions; K, thousands. (**B**) Quantitative analysis of reticulocytes of indicated mice using manual quantification of polychromatic cells in the peripheral blood. Five mice in each group were used and more than 20 representative fields were analyzed. (**C**) Histologic examination of bone marrow and spleen of the indicated mice. The histologic images are representative of 5 mice in each group analyzed. Scale bars: 100 μm. (**D**) Quantification of megakaryocytes (Meg) in the bone marrow and spleen of the indicated mice. Data were obtained from 8 mice (male and female) in each group. (**E**) Quantification of spleen/body weight ratio of the indicated mice. Data were obtained from 15 mice (male and female) in each group. *$P < 0.05$, **$P < 0.01$, ***$P < 0.0005$, and ****$P < 0.0001$; all P values were determined by 1-way ANOVA with Tukey's multiple comparisons test.

the same reduction in RBC, leukocyte, and platelet counts and rescue of JAK2^{V617F}-induced lethality (Figure 7, B and C). These results demonstrate that the role of Plek2 in mediating the pathogenesis of JAK2^{V617F}-induced MPNs is hematopoietic cell intrinsic.

Previous reports suggest that the lethality of the JAK2^{V617F} mutation could be due to thrombotic events (30, 33, 34). In humans with JAK2^{V617F}-positive MPNs, elevation of the blood cell counts correlates with an increased risk of thrombosis (33, 35, 36). Indeed, the moribund JAK2^{V617F} mice often showed signs and symptoms of thrombosis including low extremity paralysis and coolness, tachycardia, and tachypnea. We performed necropsy studies of the moribund JAK2$^{VF/+}$ Plek2$^{+/+}$ mice and indeed found widespread large vascular occlusions, which were prominent in the lungs and kidneys. In contrast, the occlusions in the same-age JAK2$^{VF/+}$ Plek2$^{-/-}$ littermate mice were significantly decreased (Figure 8A). No myelofibrosis was detected in moribund JAK2$^{VF/+}$

Plek2$^{+/+}$ mice or old (>1 year of age) JAK2$^{VF/+}$ Plek2$^{-/-}$ mice (Supplemental Figure 7A). Notably, the number of large clots (>50 μm in diameter) with compact RBC was markedly reduced in JAK2$^{VF/+}$ Plek2$^{-/-}$ mice (Figure 8B), which further implies a reduced RBC mass in these mice. Scattered small accumulations of RBC were occasionally identified in the sinusoid of JAK2$^{VF/+}$ Plek2$^{-/-}$ mice. However, these were distinct from the compact clots with many Gr1-positive granulocytes found in JAK2$^{VF/+}$ Plek2$^{+/+}$ mice (Figure 8C). We also performed a live imaging assay to detect real-time clot formation in JAK2$^{VF/+}$ Plek2$^{+/+}$ and JAK2$^{VF/+}$ Plek2$^{-/-}$ mice. Consistent with the histologic findings, widespread vascular occlusions were readily detected in JAK2$^{VF/+}$ Plek2$^{+/+}$ mice, whereas JAK2$^{VF/+}$ Plek2$^{-/-}$ mice showed relatively clear vasculature (Figure 8D). JAK2$^{VF/+}$ Plek2$^{-/-}$ mice also showed significantly improved blood flow compared with JAK2$^{VF/+}$ Plek2$^{+/+}$ mice (Figure 8E), which further supports the rescue of vascular occlusions.
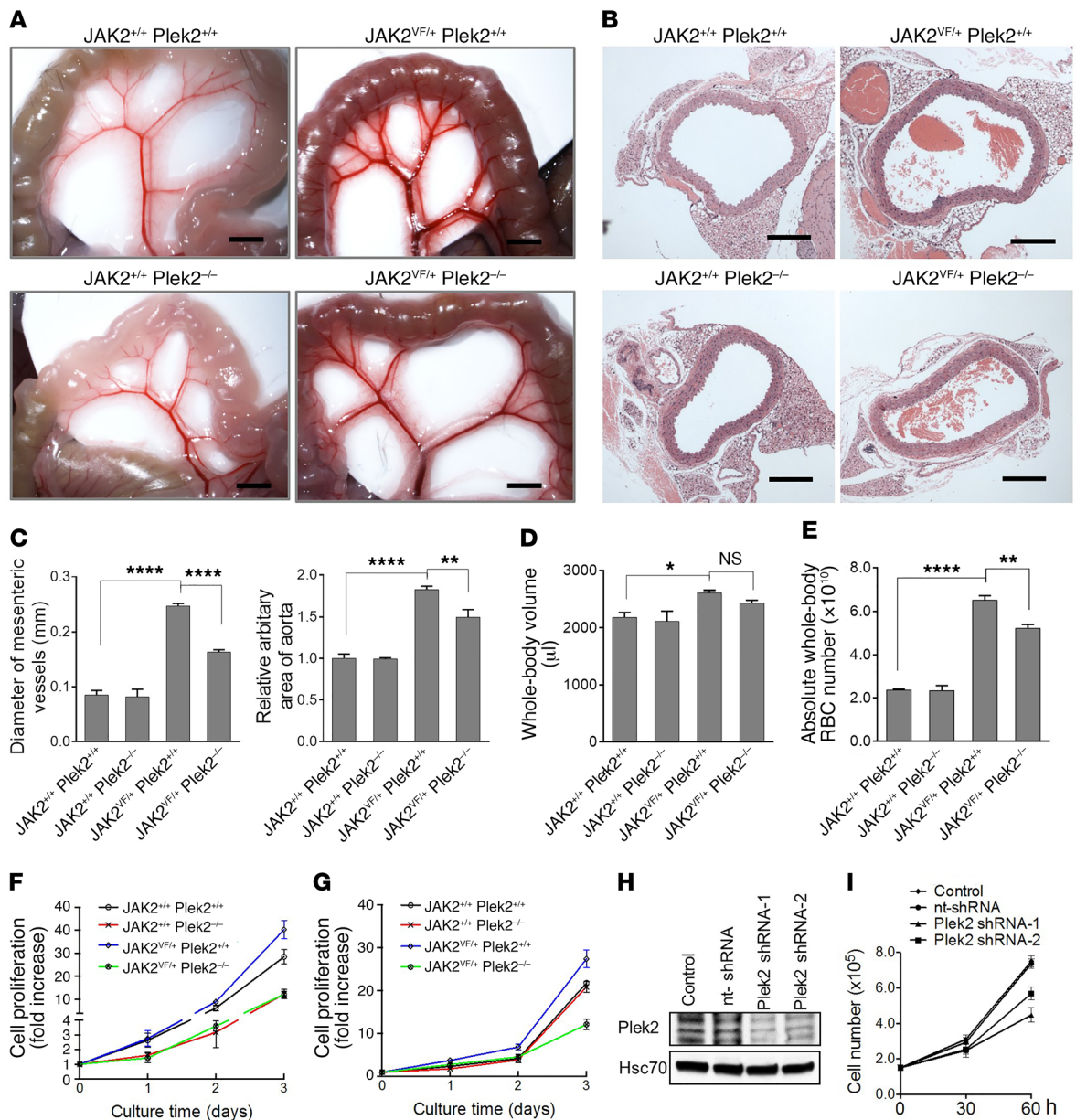
Figure 6. Reduction of RBC mass in JAK2^{V617F}-knockin mice with the loss of Plek2. (**A**) Representative mesenteric vessels at the same anatomic sites from the indicated mice. Scale bars: 2 mm. (**B**) Aorta cross section from the indicated mice. Scale bars: 200 μm. (**C**) Quantification of the diameters of the mesenteric vessels in **A** and aortic areas in **B**. $N = 5$ in each group. (**D**) Whole-body blood volume of the indicated mice. $N = 5$ in each group. (**E**) Calculated absolute circulating RBC (whole-blood volume × RBC count) of the indicated mice. $N = 5$ in each group. (**F**) Cell proliferation analyses from bone marrow lineage-negative cells of the indicated mice cultured in Epo-containing medium. Cells were counted using a hemocytometer. Data were obtained from 4 mice in each group. (**G**) Same as **C** except the cells were cultured in GM-CSF–containing medium. (**H**) Western blot assay to test the knockdown efficiency of shRNA Plek2 in SET-2 cells. Hsc70 is a loading control. (**I**) Cell proliferation assay of cells from **H** in the presence of Epo. Data were obtained from 3 independent experiments. *$P < 0.05$, **$P < 0.01$, and ****$P < 0.0001$; all P values were determined by 1-way ANOVA with Tukey's multiple comparisons test.

Reduction in RBC mass leads to the amelioration of vascular occlusion with loss of Plek2. Given previous studies indicating that the platelet count does not predict the risk of thrombosis in polycythemia vera patients (35), and the large quantity of RBC and neutrophils in the vascular occlusions in JAK2$^{VF/+}$ Plek2$^{+/+}$ mice, we tested the hypothesis that Plek2 contributes to the amelioration of vascular occlusions by reducing either the RBC mass or the number of neutrophils. To test the specific hypothesis that neutrophils are an essential mediator of the thrombotic

phenotype, we treated JAK2$^{VF/+}$ mice with repeated injections of Ly-6G antibody to reduce the peripheral neutrophil count without affecting other blood lineages (Figure 9A). Survival analysis did not detect differences between mice injected with Ly-6G antibody and those with IgG control (Figure 9B). Consistently, histologic analysis showed that the vascular occlusions were not altered by depletion of the neutrophils (Figure 9, C and D). These data suggest that the effect of Plek2 on the JAK2^{V617F} mutation is not mediated by neutrophils.
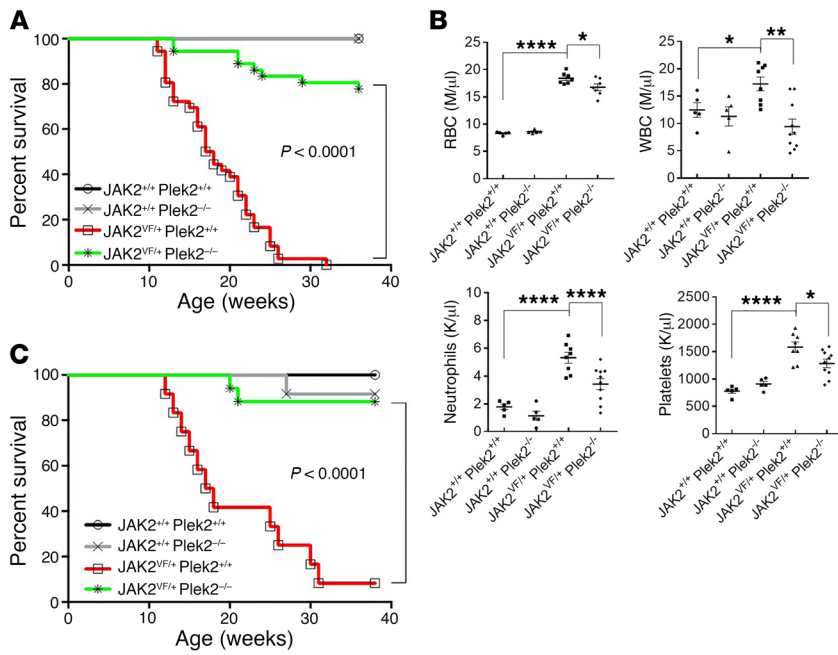
Figure 7. Loss of Plek2 rescues the lethality of the JAK2^{V617F}-knockin mice. (A) Kaplan-Meier survival analysis of indicated mice. Both males and females were included in each group. JAK2^{+/+} Plek2^{+/+} mice, $N = 34$; JAK2^{+/+} Plek2^{-/-} mice, $N = 34$; JAK2^{VF/+} Plek2^{+/+} mice, $N = 36$; JAK2^{VF/+} Plek2^{-/-} mice, $N = 36$. **(B)** Total bone marrow cells from the indicated mice (CD45.2^+, 6 weeks old) were transplanted into lethally irradiated recipient mice (CD45.1^+, 6 weeks old). Complete blood counts were performed 3 months after transplantation. Each data point represents 1 mouse. The data are shown as the mean ± SD. *$P < 0.05$, **$P < 0.01$, and ****$P < 0.0001$; all P values were determined by 1-way ANOVA with Tukey's multiple comparisons test. M, millions; K, thousands. **(C)** Kaplan-Meier survival analysis of the transplanted mice. JAK2^{+/+} Plek2^{+/+} mice, $N = 10$; JAK2^{+/+} Plek2^{-/-} mice, $N = 10$; JAK2^{VF/+} Plek2^{+/+} mice, $N = 17$; JAK2^{VF/+} Plek2^{-/-} mice, $N = 17$.

We next analyzed whether reduction of RBC with phenylhydrazine (PHZ) could mimic the Plek2 effect on JAK2^{VF/+} mice. It should be noted that PHZ reduces the RBC count without affecting neutrophils (Figure 9E). Similar to loss of Plek2, treatment with PHZ led to a reversion of JAK2^{V617F}-induced lethality (Figure 9F) as well as a marked reduction in vascular occlusion formation (Figure 9, G and H). We also analyzed whether reducing RBC counts with PHZ enhanced the protective effect of the Plek2 knockout by treating JAK2^{VF/+} Plek2^{-/-} mice with PHZ. We observed that further reduction of the RBC counts by the combination of PHZ treatment along with the Plek2 mutation led to an even greater improvement in survival (Supplemental Figure 7B). Together, these results suggest that the effect of Plek2 on reverting the JAK2^{V617F} phenotype is mediated by effects on the RBC mass.

To further understand the effect of loss of Plek2 on RBC mass and vascular occlusion formation in vivo, we repeatedly injected Epo in Plek2 wild-type and knockout mice. As expected, repeated Epo injections induced erythrocytosis in wild-type mice that was slightly less significant in Plek2-knockout mice (Figure 9I). The spleen size was also less enlarged in Plek2-knockout mice compared with wild-type ones (Figure 9J). These results suggest that loss of Plek2 leads to the reduction of whole-body RBC mass in this model. Consistent with this hypothesis, the vascular occlusions in the lungs were also less dramatic in Plek2-knockout mice compared with wild-type mice (Figure 9, K and L).

We also performed an RNA sequencing analysis of the Ter119-positive bone marrow nucleated erythroid cells in JAK2^{VF/+} Plek2^{+/+} and JAK2^{VF/+} Plek2^{-/-} mice. Consistent with the role of Plek2 in the pro-proliferative effect in terminal erythropoiesis in vivo, gene set enrichment analysis (GSEA) shows that many genes involved in cell cycle regulation are downregulated in erythroid cells from JAK2^{VF/+} Plek2^{-/-} mice compared with JAK2^{VF/+} Plek2^{+/+} ones (Supplemental Figure 8). Taken together, these data reveal that loss of Plek2-induced reduction of the RBC mass plays an important role in the amelioration of vascular occlusion and lethality in JAK2^{V617F}-knockin mice.

Discussion

In this study, we demonstrate that Plek2 is a target of the JAK2/STAT5 pathway. Given the significance of JAK2^{V617F} in the pathogenesis of the MPNs, we crossed Plek2-knockout mice with JAK2^{V617F}-knockin mice. Loss of Plek2 significantly ameliorated the myeloproliferative phenotypes and rescued JAK2^{V617F}-induced widespread vascular occlusion and lethality. These results indicate that Plek2 plays an essential role in JAK2^{V617F}-induced MPNs.

Plek2 is a widely expressed paralog of Plek1 (16). In hematopoietic cells, Plek2 exhibits strong expression levels in erythroid, granulocytic, and megakaryocytic cells. Several STAT5 consensus-binding sites are present in the promoter region of *Plek2*, which were confirmed by the ChIP assay. In contrast to Plek2, Plek1 is expressed at a low level in hematopoietic cells and its expression is not regulated by JAK2. These results indicate a hematopoietic-specific function of Plek2, in contrast with the other members of the plekstrin family.

Our previous in vitro study showed that Plek2 is important for erythroid cell survival through an interaction with cofilin. This interaction prevents cofilin's localization in mitochondria and thereby protects erythroid progenitors from cell death in the oxidative environment found in the early stage of terminal erythropoiesis (17). We were surprised that Plek2-knockout mice did not show significant anemia at a young age. It is unlikely that Plek1 compensated the defects after Plek2 deficiency since Plek1 remained at a relatively low expression level in erythroid cells. The mild anemia in old Plek2 mice and the reduced RBC survival in an oxidative environment indeed illustrate the in vivo functions of Plek2. This is further demonstrated by the increased RBC count in mice transplanted with Plek2-overexpressing bone marrow.

The significance of Plek2 in vivo is underlined when Plek2-knockout mice were crossed with JAK2^{V617F}-knockin mice. Loss of Plek2 substantially ameliorated JAK2^{V617F}-induced myeloproliferative phenotypes including leukocytosis, thrombocytosis, and partially reverted splenomegaly. Interestingly, the RBC count and
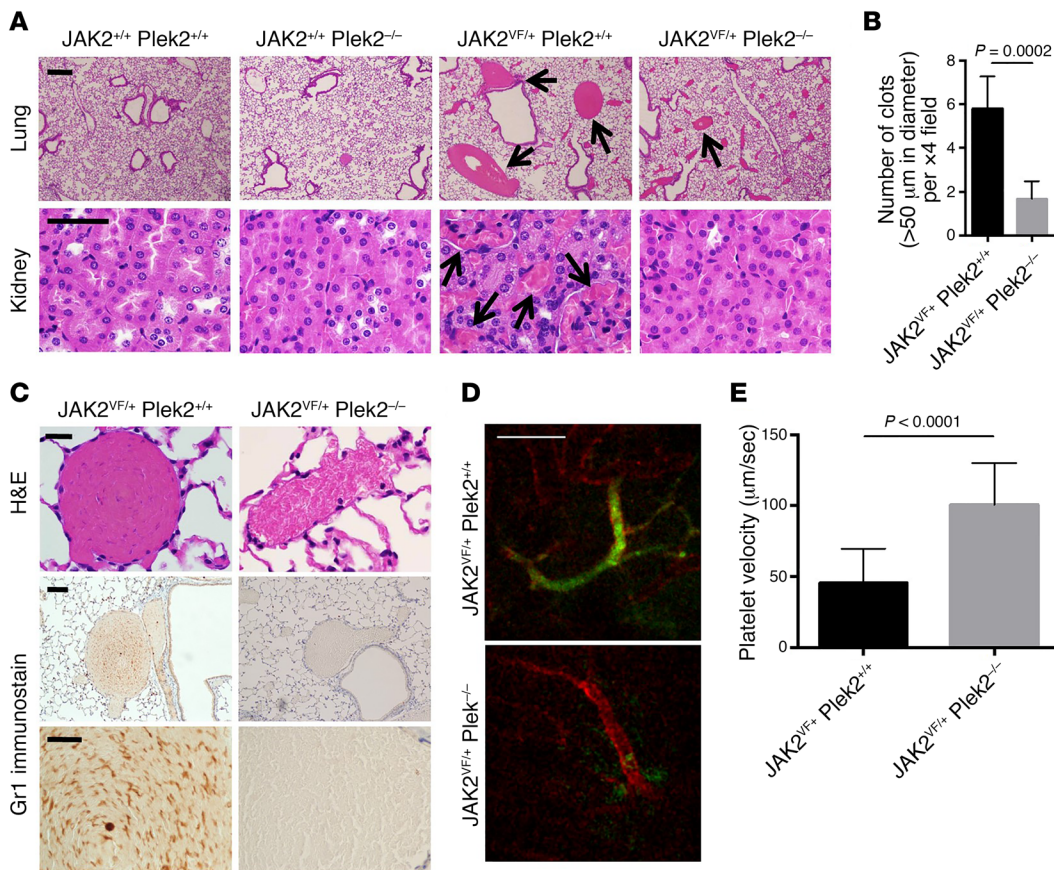
Figure 8. Loss of Plek2 reverts the vascular occlusions in the JAK2^V617F-knockin mice. (**A**) Histologic examination of the lungs and kidneys of the indicated mice. The histologic images are representative of 5 mice in each group analyzed. Arrows indicate vascular occlusions with diameters larger than 50 μm in the lungs (top panels) and numerous small occlusions in the kidneys (bottom panels). Scale bars: 100 μm. (**B**) Quantification of the number of vascular clots (>50 μm in diameter per ×4 field) in the lungs from JAK2^VF/+ Plek2^+/+ and JAK2^VF/+ Plek2^−/− mice. Fifteen fields were analyzed from 5 mice in each group. *P* value was determined by multiple 2-tailed *t* tests. (**C**) Histologic examination (H&E) and immunohistochemical stains of Gr1 to reveal granulocytes of the representative occlusions from the lungs of the indicated mice. Images are representative of 5 mice in each group analyzed. Scale bars: 20 μm. (**D**) Intravital imaging was performed on vasculature of the small intestine to examine platelet aggregation. Blood vessels and platelets were immunofluorescently stained for PECAM-1 (red) and CD41 (green), respectively. Scale bar: 100 μm. (**E**) Platelet velocity in the non-occluded area was quantified. Data were obtained from 3 independent experiments. *P* value was determined by multiple 2-tailed *t* tests.

hematocrit were not significantly reduced. This could be due to the saturated RBC production in the JAK2^V617F-knockin model. Therefore, the reduction in whole-body RBC mass may not be obviously manifested through RBC indices in peripheral blood. Indeed, we found that loss of Plek2 reduced the whole-body RBC mass indicated by the reduced spleen size and decreased vessel diameters. Reduction of whole-body circulating RBC mass in JAK2^VF/+ Plek2^−/− mice further confirmed our hypothesis. Consistent with these in vivo findings, loss of Plek2 also significantly reduced erythroid proliferation in ex vivo–cultured bone marrow lineage-negative cells and in a human JAK2 V617F–positive cell line.

One of the leading causes of mortality and mobility in MPN patients is thrombosis (33, 36). Leukocytosis, including neutrophilia, correlates with an increased risk of thrombosis in patients with MPNs (35, 36). An increased RBC mass in these patients also is well known to be contributory (37). Although loss of Plek2 normalized the total leukocyte count (including the absolute neutrophil count), depletion of leukocytes by Ly-6G injection in JAK2^V617F-knockin mice did not affect vascular occlusion or lethality. In contrast, reduction of whole-body RBC mass through PHZ injection mark-

edly reduced vascular occlusion and lethality in these mice, and phenocopied the effects with loss of Plek2. These data indicate that the reduction of vascular occlusions in JAK2^V617F-knockin mice is predominantly mediated through the reduction of the RBC mass, and not mediated via an effect on leukocytes. Our data also suggest, but do not prove that the effect of Plek2 on the survival in JAK2^VF/+ Plek2^−/− mice is independent of platelets and megakaryocytes.

Our study provides strong rationales for targeting Plek2 for the treatment of MPNs. In addition to JAK inhibitors (including the U.S. Food and Drug Administration–approved drug, ruxolitinib) (5, 6, 38–40), strategies targeting HSP90 (41), histone deacetylases (42, 43), or other cytokine receptors (44, 45) are in various stages of clinical investigation. Targeting other components of the JAK/STAT pathway makes sense given that this pathway is an essential mediator of almost all forms of Philadelphia-chromosome-negative MPNs. Several preclinical and early-stage studies are focused on combining targeting therapies against both BCL-XL and JAK2 (12, 13), STAT5 and JAK2 (14, 15), or the cell cycle–related proteins CDC25 and PIM1 (46, 47). To date, there is no evidence that inhibiting these targets enhances survival or pre-
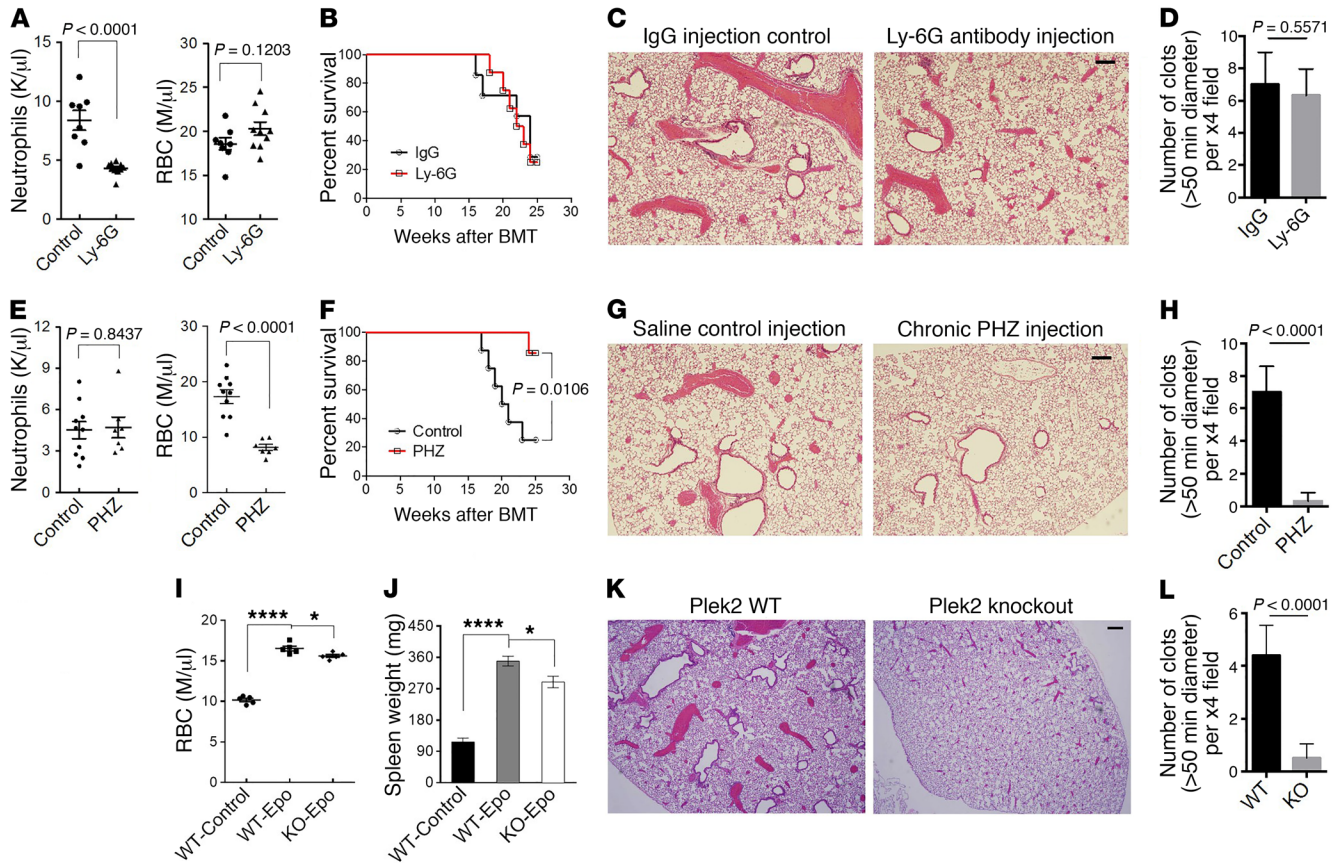
Figure 9. Reduction in RBC mass leads to the amelioration of vascular occlusion with loss of Plek2. (A) JAK2^{V617F}-knockin mice were chronically injected with Ly-6G antibody at 5 mg/kg every 3 days for 6 months. Absolute neutrophil count and RBC count in the IgG control– and Ly-6G–injected mice 2 months after injection is presented. N = 8/group. Both males and females were included in each group. K, thousands; M, millions. **(B)** Kaplan-Meier survival analysis of **A**. BMT, bone marrow transplantation. **(C)** Histologic examination of the lungs of the indicated mice. The histologic images are representative of 5 mice in each group analyzed. **(D)** Quantification of the number of vascular occlusions (>50 μm in diameter per ×4 field) in the lungs from the indicated mice. Fifteen fields were analyzed from 5 mice in each group. **(E–H)** Same as **A**–**D** except that the mice were chronically injected with PHZ at 25 mg/kg every 3 days for 6 months. N = 8/group. **(I)** Wild-type or Plek2-knockout mice were chronically injected with erythropoietin at 5,000 U/kg every 2 days for 3 weeks. RBC counts were analyzed 3 weeks after injection. N = 6/group. **(J)** Spleen weight of the mice from **I**. **(K)** Histologic examination of the lungs of the indicated mice. The histologic images are representative of 5 mice in each group analyzed. **(L)** Quantification of the number of vascular occlusions as in **D**. *P < 0.05 and ****P < 0.0001, by 1-way ANOVA with Tukey's multiple comparisons test. All scale bars: 100 μm.

vents thrombosis. Therefore, targeting a novel JAK/STAT effector, Plek2, to treat MPNs has both rationale and appeal. Since Plek2 is also a downstream target of PI3K (48), which is also activated in MPNs (44), Plek2 could also serve as a node for the dual targeting of JAK2 and PI3K pathways.

One of the major side effects of JAK inhibitors is myelosuppression (6). Plek2-knockout mice were largely normal at the young age and only showed mild anemia when the mice were more than 1 year of age. However, loss of Plek2 showed suppressive effects in the myeloid cells specifically in the JAK2^{V617F}-positive background. These phenotypes were also transplantable, indicating cell-intrinsic effects. These results suggest that targeting Plek2 for the treatment of MPN may be specific for JAK2^{V617F}-mutant clones but less influential on normal hematopoiesis.

Overall, our work adds to existing evidence that an increased RBC mass plays a critical role in thrombosis in JAK2^{V617F}-induced MPNs. More importantly, this study reveals that Plek2 is an effector of JAK2 signaling, and is critical for the pathogenesis of JAK2^{V617F}-induced MPNs. Loss of Plek2 substantially reduces vascular occlu-

sion and lethality mainly through the reduction of RBC mass. These findings provide a proof of principle that Plek2 is a potential mediator of MPNs and a viable target for their treatment.

Methods

Mice. C57BL/6 mice used for the fetal liver erythroblasts and bone marrow lineage-negative cell purification were purchased from The Jackson Laboratory. JAK2^{V617F} floxed (JAK2$^{VF/+}$) conditional knockin mice (C57BL/6 background) were provided by Benjamin Ebert and Ann Mullally (Harvard Medical School, Boston, Massachusetts, USA).

To generate Plek2-knockout mice, a 10.6-kb genomic DNA fragment, isolated from a 129SV agouti mouse strain library containing exon 3 of the Plek2 gene, was used to generate the gene-targeting vector. This exon was replaced with a neomycin-resistance gene in the plasmid. The gene-targeting construct was transfected into R1 embryonic stem (ES) cells by electroporation. After selection with Geneticin, a recombinant ES cell clone was microinjected into blastocysts, and chimeras were generated. These chimeras then were backcrossed with C57BL6 mice to produce heterozygotes. Finally,

interbreeding of heterozygous siblings yielded animals homozygous for the desired mutation, i.e., mice lacking Plek2.

To generate hematopoietic-specific JAK2^{V617F}-knockin mice, we crossed *Vav-Cre* mice with Plek2-knockout mice or JAK2$^{VF/+}$ mice to generate Vav-Cre Plek2$^{+/+}$, Vav-Cre Plek2$^{-/-}$, and Vav-Cre JAK2$^{VF/+}$ mice. Next we crossed Vav-Cre Plek2$^{+/+}$ and Vav-Cre Plek2$^{-/-}$ mice with Vav-Cre JAK2$^{VF/+}$ mice and obtained the following 4 genotypes: JAK2$^{+/+}$ Plek2$^{+/+}$, JAK2$^{+/+}$ Plek2$^{-/-}$, JAK2$^{VF/+}$ Plek2$^{+/+}$, and JAK2$^{VF/+}$ Plek2$^{-/-}$ mice (all carrying Vav-Cre). For the survival assay, these mice were monitored biweekly and were sacrificed when moribund. Statistical analysis was performed with Prism (GraphPad Software) via the Kaplan-Meier method. For the analyses of complete blood counts, peripheral blood (70 μl from each mouse) was collected from the retro-orbital vein in EDTA-coated tubes and analyzed by a Hemavet 950 complete blood counter (Drew Scientific).

Human recombinant Epo was obtained from Northwestern Memorial Hospital (Chicago, Illinois, USA). Wild-type mice were treated with Epo (5,000 U/kg body weight) or saline control every 2 days for 3 weeks. Anti–mouse Ly-6G antibody (catalog BP0075) and IgG control were obtained from BioXCell. JAK2^{V617F}-knockin mice were treated with Ly-6G (5 mg/kg body weight) or IgG every 3 days for 6 months. For the PHZ treatment, JAK2^{V617F}-knockin mice were treated with 25 mg/kg body weight every 3 days for 6 months. All the treatments were performed by intraperitoneal injection. For the pathologic examination, mice were euthanized with CO_2 and tissue organs were dissected. The sternum, spleen, liver, kidney, brain, heart, and intestine were collected. The lungs were dissected after perfusion with formalin via the tracheobronchial tree. All organs were fixed in 4% neutral buffered formalin and embedded in paraffin for histological and pathological examination.

Cell culture. Purification of mouse fetal liver erythroblast precursors (CFU-E; Ter119-negative cells) and in vitro culture were performed as previously described (17). Briefly, fetal liver cells were isolated from E13.5 C57BL/6 embryos and mechanically dissociated by pipetting in phosphate-buffered saline (PBS) containing 10% FBS (Gemini). Single-cell suspensions were prepared by passing the dissociated cells through 40-μm cell strainers (BD Biosciences). Total fetal liver cells were labeled with biotin-conjugated anti-Ter119 antibody (1:100) (eBioscience, catalog 13-5921-82), and Ter119-negative cells were purified using an EasySep column free cell isolation system according to the manufacturer's instructions (Stem Cell Technologies). Purified cells were cultured in Iscove's modified Dulbecco's medium (IMDM) containing 15% FBS (Stem Cell Technologies), 1% detoxified BSA (Stem Cell Technologies), 200 μg/ml holo-transferrin (MilliporeSigma), 10 μg/ml recombinant human insulin (MilliporeSigma), 2 mM L-glutamine, 10^{-4} M β-mercaptoethanol, and 2 U/ml recombinant human Epo (Amgen).

Bone marrow cells were isolated from the hind legs of C57BL/6 mice aged 6–8 weeks and were mechanically dissociated by pipetting in PBS containing 2% FBS. Progenitor cells were enriched by lineage-negative selection using a progenitor cell enrichment kit (Stem Cell Technologies) according to the manufacturer's instructions. For erythroblast differentiation, the purified bone marrow progenitor cells were cultured as fetal liver erythroblast precursors mentioned above. For granulocytic differentiation, the purified bone marrow progenitor cells were cultured in a myeloid differentiation medium for 3 days (IMDM containing 15% FBS, 0.1 mM β-mercaptoethanol, 1% penicillin-streptomycin, 2 mM L-glutamine, 50 ng/ml mouse SCF [PeproTech], 10 ng/ml IL-3 [PeproTech], and 10 ng/ml granulocyte macrophage

colony-stimulating factor [PeproTech]). For megakaryocytic differentiation, the purified bone marrow progenitor cells were first cultured in StemSpan (Stem Cell Technologies) supplemented with 10 ng/ml murine IL-3 (PeproTech), 10 ng/ml human IL-6 (PeproTech), 40 ng/ml murine SCF, and 10 μg/ml human low density lipoprotein (Stem Cell Technologies) for 3 days. The cells were then maintained in RPMI 1640 medium with 10% FBS, 20 ng/ml murine thrombopoietin, and 10 ng/ml murine SCF.

Flow cytometric assays. Bone marrow cells were obtained as described above. Spleen cells were prepared by pipetting and passing the tissue through a 70-μm cell strainer (BD Biosciences). Single-cell suspensions of bone marrow, spleen, or cultured cells were prepared by resuspending the cells in PBS with 0.5% BSA (Santa Cruz Biotechnology) and 2 mM EDTA (Gibco). Cells were immunostained with the following antibodies purchased from eBioscience: CD71 (catalog 11-0711), Ter119 (catalog 17-5921), CD44 (catalog 12-0441), CD45.2 (catalog 48-0454), B220 (catalog 17-0452), Gr-1 (catalog 48-5931), CD41 (catalog 11-0411), CD11b (catalog 17-0112), and CD3e (catalog 48-032). Propidium iodide was added to exclude dead cells from analysis. All staining was performed for 20 minutes at room temperature. The samples were analyzed on a FACSCalibur flow cytometer (BD Biosciences). Postacquisition analyses were performed with FlowJo software V9.2.3 (Tree Star).

Generation of retroviral particles and transduction of primary cells. Retroviral constructs MSCV-IRES-GFP-STAT5 wild-type, dominant-negative, and constitutively active mutants were provided by Merav Socolovsky of the University of Massachusetts Medical School. MSCV-IRES-GFP-JAK2 wild-type and V617F mutant were provided by Lily Huang of the University of Texas Southwestern Medical Center (Dallas, Texas, USA). For the generation of retroviral particles, HET293T cells were plated on 10-cm culture dishes overnight, followed by transfection with the plasmids mentioned above and the retroviral packaging construct Pcl-Eco in a 2:1 ratio by TransIT-LT1 transfection reagent (Mirus) according to the manufacturer's protocols. Viral supernatants were collected after 48 hours. To perform retroviral infection of the purified Ter119-negative mouse fetal liver cells or bone marrow lineage-negative cells, the cells were resuspended in viral supernatants with 8 μg/ml polybrene (MilliporeSigma) and centrifuged at 1,800 rpm for 1 hour at 37°C. After spin-infection, the viral supernatants were immediately removed and fresh media were added.

Quantitative real-time RT-PCR. Total RNA from fetal liver cells, bone marrow cells, or cultured cells was purified with TRIzol (Invitrogen). cDNA was reverse transcribed from 1 μg total RNA with random primers using Superscript III (Invitrogen), as described by the manufacturer. Quantitative RT-PCR was performed using PerfeCTa SYBR Green QPCR FastMix ROX (Quanta Biosciences, Inc.) according to the manufacturer's protocols. The primers used for the PCR were *Plek2*-forward, AAAGACCTTTCTGGGCTCCT; *Plek2*-reverse, CCCTACTGGCCTGAGAAAGT; 18S rRNA-forward, GCAATTATTCCCCATGAACG; and 18S rRNA-reverse, GGCCTCACTAAACCATCCAA. Fluorescence was detected in an ABI StepOnePlus (Applied Biosystems). Cycle threshold (Ct) values were calculated by the ABI StepOnePlus software. Relative gene expression levels were expressed as the difference in Ct values (ΔCt) of the target gene and the housekeeping gene (18S rRNA, eukaryotic 18S ribosomal RNA) in each sample, and normalized to 18S rRNA expression. All PCRs were performed in triplicate.

Luciferase reporter assay. A 2,000-bp fragment (bases −1 to −2000) of the mouse *Plek2* promoter was amplified by PCR (forward primer, 5′-AAGGGTACCGCACGATTTCTTCCAATGCCCT-3′; reverse primer, 5′-ATTCTCGAGGCGCACATCCAGTGCCAGAGCC-3′) and ligated into a pGL3 luciferase reporter vector (Promega). HET293T cells were cotransfected with the *Plek2* luciferase reporter construct and MSCV-IRES-GFP-STAT5 constructs using TransIT-LT1 transfection reagent (Mirus) according to the manufacturer's protocols. Cells were harvested 24 hours after transfection, and luciferase activity was measured using the Dual-Promoter Luciferase Assay Kit (Promega) and firefly luciferase was normalized to *Renilla* luciferase.

ChIP assay. ChIP was performed with a SimpleChIP Enzymatic Chromatin IP Kit (Cell Signaling Technology, 9002) according to the manufacturer's protocol. Crossed chromatin (10–15 μg) was immunoprecipitated with 3 μg of anti-STAT5 (Santa Cruz Biotechnology, sc-835) or anti-histone H3 (Cell Signaling Technology, 4620) antibody. An equal amount of normal rabbit IgG (Cell Signaling Technology, 2729) was used as the control. The recovered DNA was analyzed by real-time PCR as described above using the following primers specific for different domains of the *Plek2* promoter: P1 (forward and reverse), TGACAGACCATGAACCATCC and GCTCAGGTACTGGGTTTGGT; P2, CCAGGCTTCTTCCAGTTCTC and AGGCTGTGTCATCTGTCAGG; P3, TGGAACCAGAGTTACAGGCA and TTTCCAGAGGACCTGGATTT; P4, GCTTTGAGACTTGTCTTGCCT and CACAATGAGCACTTTGGCTT; P5, TGGAGGTTCCTTCCTCCTC and ATGACTGCACCACCAACCTA; P6, GGTATTCGGAAGCACGATTT and CCAGGAGGCAAATAATGTGTT; P7, CCTAGCAGGTGTTCCCTCTG and GTTGGCACCTGAAACAAGAA. Signals obtained from each immunoprecipitation are presented as the percentage of the total input chromatin.

Western blot analyses. Cell were lysed in ice-cold RIPA buffer (50 mM Tris-HCl [pH 7.4], 150 mM NaCl, 1 mM EDTA, 1% NP-40, and 0.25% sodium deoxycholate) with protease inhibitors (Protease Inhibitor Cocktail Tablets, Roche). Proteins were separated by SDS-PAGE (Bio-Rad) and transferred to Immobilon-P membranes (MilliporeSigma) and immunoblotted using the following antibodies: anti-Plek2 (Proteintech, 11685-1-AP), anti-STAT5 (Santa Cruz Biotechnology, sc-835), anti-p-STAT5 (Cell Signaling Technology, 9359), and anti-Hsc70 (Santa Cruz Biotechnology, sc-7298). See complete unedited blots in the supplemental material.

Plek2 gene expression profiling of patients. Two reported data sets of global gene expression profiling in JAK2^{V617F}-positive patients were used to examine the expression levels of Plek2 (see figure legends for details). Relative gene expression levels of Plek2 in bone marrow samples derived from 16 JAK2^{V617F}-positive polycythemia vera patients and 9 JAK2^{V617F}-positive essential thrombocythemia patients were normalized to the mean of that in the corresponding 26 healthy controls. Peripheral blood samples from JAK2^{V617F}-positive MPN patients and healthy individuals were obtained from Northwestern Memorial Hospital. Mononuclear cells were purified from these samples followed by total RNA extraction. Relative Plek2 gene expression levels were analyzed by real-time PCR as above described. Western blot analysis was also performed for Plek2 protein expression.

Intravital imaging. Mice were anesthetized by intraperitoneal injection of ketamine and xylazine solution (100 mg/kg and 5 mg/kg, respectively). A small piece of the small intestine was gently exteriorized and placed on a custom-designed platform, superfused with warmed physiological solution. Mouse core body temperature was maintained by placing the mouse on a warming pad set to 37°C. Imaging experiments were performed using an Ultraview Vox imaging system equipped with 488, 561, and 640 nm laser lines, a Nipkow disk confocal head (CSU 10, Yokogawa Yokogawa Electric) attached to an intensified CCD camera and a 20× water-immersion objective (NA = 1.00). Laser power and camera gain settings were unchanged throughout all the experiments. Images were digitally acquired at a resolution of 512 × 512 pixels using Velocity software (PerkinElmer) and analyzed using ImageJ (NIH). A mix of anti–PECAM-1 (eBioscience, catalog 12-0311-82) and anti-CD41 (eBioscience, catalog 11-0411-82) monoclonal antibodies conjugated to Alexa 555 and Alexa 488 (2 μg/ml), respectively, were injected via the tail vain at the beginning of the imaging protocols to outline the intestinal blood vessels and platelets. Platelet velocity was calculated as cell displacement in an axial direction over time.

Bone marrow transplantation. Bone marrow cells from JAK2$^{VF/+}$ Plek2$^{+/+}$ and JAK2$^{VF/+}$ Plek2$^{-/-}$ mice as well as their littermate controls (CD45.2-positive, 8–10 weeks old) were extracted and a total of 2×10^6 cells were transplanted into lethally irradiated (10 Gy) recipient mice (CD45.1-positive, B6-LY-5.2/Cr). Recipient mice were then kept on antibiotic water (1.1 mg/ml neomycin and 2,000 U/ml polymyxin B [both MilliporeSigma]) for 2 weeks, followed by regular water. Bone marrow engraftment was determined by flow cytometric analysis for the ratio of CD45.1-positive recipient-derived and CD45.2-positive donor-derived cells in the peripheral blood of recipient mice. For Plek2 overexpression bone marrow transplantation, hematopoietic stem and progenitor cells (HSPCs) were purified from wild-type mice (CD45.2-positive, 6–8 weeks old) bone marrow using a c-kit$^+$ selection kit (Stem Cell Technologies, catalog 18757), and cultured in expansion medium overnight. Viral transduction was performed twice on the second day. The cells (1×10^6) were then transplanted into lethally irradiated recipient mice (CD45.1-positive, B6-LY-5.2/Cr).

Bone marrow neutrophil purification and transwell migration assay. Bone marrow cells were isolated by flushing femurs and tibias of 8- to 10-week-old mice with Ca/Mg–free PBS containing 2% FBS. Neutrophils were enriched by depletion of stem cells/progenitor cells (CD117$^+$) and other lineage-positive cells (CD71$^+$, TER119$^+$, CD3$^+$, B220$^+$, and CD41$^+$). This procedure routinely yielded greater than 90% neutrophils as determined by flow cytometry. The purified neutrophils were suspended in Ca/Mg–free HBSS containing 2 mg/ml BSA. A 50-μl cell suspension (3×10^5 cells) was placed in the upper compartment of a transwell chamber featuring 5-μm pores in an uncoated polycarbonate membrane (Corning), and 250 μl HBSS containing 2 mg/ml BSA with 100 nm *N*-formyl-methionyl-leucyl-phenylalanine (MilliporeSigma, catalog F3506) or vehicle was added to the bottom chamber. After incubation for 2.5 hours at 37°C and 5% CO$_2$, the cells in the lower chamber were harvested and counted.

Platelet aggregation and dense granule secretion assays. Washed platelets were used for the assay. The concentration of platelets was adjusted to 2×10^8 platelets/ml by using Hepes–Tyrode's buffer and supplemented with 1 mM CaCl$_2$. Various concentrations of thrombin or collagen were added to the washed platelets. Platelet aggregation was measured by the turbidometric method at 37°C in the presence of Chrono-Lume luciferase in a Lumi-Dual aggregometer (Chrono-Log).

RNA-sequencing gene expression profiling and GSEA. TER119-positive erythroid cells were purified from 3-month-old JAK2$^{VF/+}$ Plek2$^{+/+}$ and JAK2$^{VF/+}$ Plek2$^{-/-}$ bone marrow. Total RNA was extract-

ed using the TRIzol reagent following the manufacturer's recommendations (Invitrogen). RNA quality and quantity was determined using an Agilent Bio-analyzer. RNA-sequencing libraries were generated using an Illumina TruSeq Stranded mRNA kit as instructed by the manufacturer. Libraries were quantified using an Agilent Bio-analyzer. Sequencing was performed using an Illumina HiSEQ4000 with Illumina-provided reagents and protocols. RNA-sequencing data were deposited in the NCBI's Gene Expression Omnibus database (GEO GSE97658).

The GSEA was performed using the RNA-sequencing gene expression profiling data and GSEA software and the Molecular Signatures Database (Broad Institute, Cambridge, Massachusetts, USA).

Calculation of circulating RBC mass in mice. Plasma volume was measured using a modified Evans blue dye (EBD) method described previously (49, 50). Briefly, an initial (blank) blood sample of 100 μl was withdrawn from the orbital sinus followed by injection of 50 μl of 0.2% EBD (MilliporeSigma, catalog E2129) solution in normal saline through intravenous injection. Blood samples (500 μl) were collected at 10 and 20 minutes after injection. All samples were collected in EDTA-coated vacutainers. These blood samples were analyzed by a Hemavet 950 complete blood counter (Drew Scientific). Plasma was then separated from the whole-blood samples. The EBD content in each plasma sample was determined by means of absorbance read at 650 nm, and was calculated from a standard solution in pooled plasma of mice. Plasma volume (V) was calculated as $V = C_{inject} \times V_{inject}/C_{sample}$, where C_{inject} = EBD concentration of injected EBD; V_{inject} = volume of injected EBD; C_{sample} = measured concentration of EBD in the sample of plasma. Whole-body blood volume was calculated from measured plasma volume and hematocrit (Hct) that was obtained from the complete blood counter: Blood Volume = Plasma Volume/(1 – Hct). Estimation of circulating RBC mass was obtained from the equation, Whole-body Blood Volume × RBC, where RBC = red blood cell (erythrocyte) count.

Statistics. The analysis of results was performed using Prism 6 (GraphPad Software). All data are presented as mean ± SD except where indicated otherwise. Statistical differences between 2 groups were evaluated using a 2-tailed *t* test. Multiple group comparisons were performed using a 1-way ANOVA followed by Dunnett's or Tukey's post test except where indicated otherwise. A *P* value of less than 0.05 was considered statistically significant.

Study approval. All animal studies were performed in accordance with the NIH Guidelines for the Care and Use of Laboratory Animals and were approved by the Institutional Animal Care and Use Committees at Northwestern University, Chicago, Illinois. MPN patient data were obtained following informed consent under Institutional Review Board–approved protocols at Northwestern University, Chicago, Illinois.

Author contributions

Acknowledgments

Address correspondence to: Peng Ji, Department of Pathology, Feinberg School of Medicine, Northwestern University, 303 East Chicago Avenue, Ward 3-230, Chicago, Illinois 60611, USA. Phone: 312.503.3191; Email: ji.peng@northwestern.edu.

1. Levine RL, et al. Activating mutation in the tyrosine kinase JAK2 in polycythemia vera, essential thrombocythemia, and myeloid metaplasia with myelofibrosis. *Cancer Cell*. 2005;7(4):387–397.

2. Kralovics R, et al. A gain-of-function mutation of JAK2 in myeloproliferative disorders. *N Engl J Med*. 2005;352(17):1779–1790.

3. James C, et al. A unique clonal JAK2 mutation leading to constitutive signalling causes polycythaemia vera. *Nature*. 2005;434(7037):1144–1148.

4. Baxter EJ, et al. Acquired mutation of the tyrosine kinase JAK2 in human myeloproliferative disorders. *Lancet*. 2005;365(9464):1054–1061.

5. Cervantes F, et al. Three-year efficacy, safety, and survival findings from COMFORT-II, a phase 3 study comparing ruxolitinib with best available therapy for myelofibrosis. *Blood*. 2013;122(25):4047–4053.

6. Harrison C, et al. JAK inhibition with ruxolitinib versus best available therapy for myelofibrosis. *N Engl J Med*. 2012;366(9):787–798.

7. Sonbol MB, Firwana B, Zarzour A, Morad M, Rana V, Tiu RV. Comprehensive review of JAK inhibitors in myeloproliferative neoplasms. *Ther Adv Hematol*. 2013;4(1):15–35.

8. Nangalia J, Grinfeld J, Green AR. Pathogenesis of myeloproliferative disorders. *Annu Rev Pathol*. 2016;11:101–126.

9. Rampal R, et al. Integrated genomic analysis illustrates the central role of JAK-STAT pathway activation in myeloproliferative neoplasm pathogenesis. *Blood*. 2014;123(22):e123–e133.

10. Tefferi A, Pardanani A. Myeloproliferative neoplasms: a contemporary review. *JAMA Oncol*. 2015;1(1):97–105.

11. Elf S, et al. Mutant calreticulin requires both its mutant C-terminus and the thrombopoietin receptor for oncogenic transformation. *Cancer Discov*. 2016;6(4):368–381.

12. Waibel M, et al. Combined targeting of JAK2 and Bcl-2/Bcl-xL to cure mutant JAK2-driven malignancies and overcome acquired resistance to JAK2 inhibitors. *Cell Rep*. 2013;5(4):1047–1059.

13. Lu M, et al. Treatment with the Bcl-xL inhibitor ABT-737 in combination with interferon α specifically targets JAK2V617F-positive polycythemia vera hematopoietic progenitor cells. *Blood*. 2010;116(20):4284–4287.

14. Nelson EA, et al. The STAT5 inhibitor pimozide decreases survival of chronic myelogenous leukemia cells resistant to kinase inhibitors. *Blood*. 2011;117(12):3421–3429.

15. Bar-Natan M, Nelson EA, Walker SR, Kuang Y, Distel RJ, Frank DA. Dual inhibition of Jak2 and STAT5 enhances killing of myeloproliferative neoplasia cells. *Leukemia*. 2012;26(6):1407–1410.

16. Hu MH, Bauman EM, Roll RL, Yeilding N, Abrams CS. Pleckstrin 2, a widely expressed paralog of pleckstrin involved in actin rearrangement. *J Biol Chem*. 1999;274(31):21515–21518.

17. Zhao B, et al. Targeted shRNA screening identified critical roles of pleckstrin-2 in erythropoiesis. *Haematologica*. 2014;99(7):1157–1167.

18. Ji P, Jayapal SR, Lodish HF. Enucleation of cultured mouse fetal erythroblasts requires Rac GTPases and mDia2. *Nat Cell Biol*. 2008;10(3):314–321.

19. Ji P, Murata-Hori M, Lodish HF. Formation of mammalian erythrocytes: chromatin condensation and enucleation. *Trends Cell Biol*. 2011;21(7):409–415.

20. Liu J, et al. Quantitative analysis of murine terminal erythroid differentiation in vivo: novel method to study normal and disordered erythropoiesis. *Blood*. 2013;121(8):e43–e49.

21. Witthuhn BA, et al. JAK2 associates with the erythropoietin receptor and is tyrosine phosphorylated and activated following stimulation with erythropoietin. *Cell*. 1993;74(2):227–236.

22. Corces MR, et al. Lineage-specific and single-cell chromatin accessibility charts human hematopoiesis and leukemia evolution. *Nat Genet*. 2016;48(10):1193–1203.

23. Chen E, et al. Distinct clinical phenotypes associated with JAK2V617F reflect differential STAT1 signaling. *Cancer Cell*. 2010;18(5):524–535.

24. Berkofsky-Fessler W, et al. Transcriptional profiling of polycythemia vera identifies gene expression patterns both dependent and independent from the action of JAK2V617F. *Clin Cancer Res*. 2010;16(17):4339–4352.

25. Goerttler PS, et al. Gene expression profiling in polycythaemia vera: overexpression of transcription factor NF-E2. *Br J Haematol*. 2005;129(1):138–150.

26. Kralovics R, et al. Altered gene expression in myeloproliferative disorders correlates with activation of signaling by the V617F mutation of Jak2. *Blood*. 2005;106(10):3374–3376.

27. Pellagatti A, et al. Gene expression profiling in polycythemia vera using cDNA microarray technology. *Cancer Res*. 2003;63(14):3940–3944.

28. Puigdecanet E, et al. Gene expression profiling distinguishes JAK2V617F-negative from JAK2V617F-positive patients in essential thrombocythemia. *Leukemia*. 2008;22(7):1368–1376.

29. Tenedini E, et al. Gene expression profiling of normal and malignant CD34-derived megakaryocytic cells. *Blood*. 2004;104(10):3126–3135.

30. Mullally A, et al. Physiological Jak2V617F expression causes a lethal myeloproliferative neoplasm with differential effects on hematopoietic stem and progenitor cells. *Cancer Cell*. 2010;17(6):584–596.

31. Kleppe M, et al. JAK-STAT pathway activation in malignant and nonmalignant cells contributes to MPN pathogenesis and therapeutic response. *Cancer Discov*. 2015;5(3):316–331.

32. Lamrani L, et al. Hemostatic disorders in a JAK2V617F-driven mouse model of myeloproliferative neoplasm. *Blood*. 2014;124(7):1136–1145.

33. Elliott MA, Tefferi A. Thrombosis and haemorrhage in polycythaemia vera and essential thrombocythaemia. *Br J Haematol*. 2005;128(3):275–290.

34. Akada H, Yan D, Zou H, Fiering S, Hutchison RE, Mohi MG. Conditional expression of heterozygous or homozygous Jak2V617F from its endogenous promoter induces a polycythemia vera-like disease. *Blood*. 2010;115(17):3589–3597.

35. Falanga A, Marchetti M. Thrombosis in myeloproliferative neoplasms. *Semin Thromb Hemost*. 2014;40(3):348–358.

36. Barbui T, Finazzi G, Falanga A. Myeloproliferative neoplasms and thrombosis. *Blood*. 2013;122(13):2176–2184.

37. Adams BD, Baker R, Lopez JA, Spencer S. Myeloproliferative disorders and the hyperviscosity syndrome. *Hematol Oncol Clin North Am*. 2010;24(3):585–602.

38. Verstovsek S, et al. Efficacy, safety, and survival with ruxolitinib in patients with myelofibrosis: results of a median 3-year follow-up of COMFORT-I. *Haematologica*. 2015;100(4):479–488.

39. Pasquier F, Cabagnols X, Secardin L, Plo I, Vainchenker W. Myeloproliferative neoplasms: JAK2 signaling pathway as a central target for therapy. *Clin Lymphoma Myeloma Leuk*. 2014;14 Suppl:S23–S35.

40. Pardanani A, et al. Safety and efficacy of CYT387, a JAK1 and JAK2 inhibitor, in myelofibrosis. *Leukemia*. 2013;27(6):1322–1327.

41. Marubayashi S, et al. HSP90 is a therapeutic target in JAK2-dependent myeloproliferative neoplasms in mice and humans. *J Clin Invest*. 2010;120(10):3578–3593.

42. Rambaldi A, et al. A pilot study of the histone-deacetylase inhibitor Givinostat in patients with JAK2V617F positive chronic myeloproliferative neoplasms. *Br J Haematol*. 2010;150(4):446–455.

43. Guerini V, et al. The histone deacetylase inhibitor ITF2357 selectively targets cells bearing mutated JAK2(V617F). *Leukemia*. 2008;22(4):740–747.

44. Bartalucci N, et al. Co-targeting the PI3K/mTOR and JAK2 signalling pathways produces synergistic activity against myeloproliferative neoplasms. *J Cell Mol Med*. 2013;17(11):1385–1396.

45. Guglielmelli P, et al. Safety and efficacy of everolimus, a mTOR inhibitor, as single agent in a phase 1/2 study in patients with myelofibrosis. *Blood*. 2011;118(8):2069–2076.

46. Gautier EF, et al. The cell cycle regulator CDC25A is a target for JAK2V617F oncogene. *Blood*. 2012;119(5):1190–1199.

47. Wernig G, et al. The Jak2V617F oncogene associated with myeloproliferative diseases requires a functional FERM domain for transformation and for expression of the Myc and Pim proto-oncogenes. *Blood*. 2008;111(7):3751–3759.

48. Bach TL, et al. PI3K regulates pleckstrin-2 in T-cell cytoskeletal reorganization. *Blood*. 2007;109(3):1147–1155.

49. Armin J, Grant RT, Pels H, Reeve EB. The plasma, cell and blood volumes of albino rabbits as estimated by the dye (T 1824) and ^{32}P marked cell methods. *J Physiol (Lond)*. 1952;116(1):59–73.

50. Baby PM, et al. A novel method for blood volume estimation using trivalent chromium in rabbit models. *Indian J Plast Surg*. 2014;47(2):242–248.